Decoding human placental cellular and molecular responses to maternal obesity and fetal growth

Hong Jiang[1†], Emilie Derisoud[1†], Denise Parreira[2], Nayere Taebnia[1,3], Paulo R. Jannig[1], Reza Zandi Shafagh[1,3,6], Allan Zhao[1], Congru Li[1], Macarena Ortiz[5], Manuel Alejandro Maliqueo[5], Elisabet Stener-Victorin[1], Volker M. Lauschke[1,3,4,7], Qiaolin Deng[1,2,*]

[1]Karolinska Institutet, Department of Physiology and Pharmacology, Stockholm, 17177, Sweden

[2]Stockholm University, Department of Molecular Biosciences, the Wenner-Gren Institute, 10691, Sweden

[3]Center for Molecular Medicine, Karolinska Institutet and University Hospital, Stockholm, 17176 Sweden

[4]Dr Margarete Fischer-Bosch Institute of Clinical Pharmacology, Stuttgart, 70376, Germany

[5]University of Chile, Departamento de Medicina Interna, Santiago, 8330015, Chile

[6]Division of Micro- and Nanosystems, KTH Royal Institute of Technology, Stockholm, Sweden

[7]Department of Pharmacy, the Second Xiangya Hospital, Central South University, Changsha, China

[†] These authors have contributed equally to this work and share first authorship

* Corresponding Author: qiaolin.deng@ki.se (ORCID ID: 0000-0001-5934-7816)

Abstract

Obesity poses risks to maternal health and increases the likelihood of short- and long-term adverse pregnancy outcomes in the offspring. The placenta, a key organ at the maternal-fetal interface, responds to maternal obesity and regulates fetal growth. To investigate the molecular features of physiological adaptation, we perform single-nuclei RNA-seq on human placentas and compared the transcriptomic profiles of women with obesity delivering appropriate- or large-for-gestational age (i.e., AGA and LGA) babies with those from normal-weight healthy controls delivering AGA babies. Commonness-score metric is developed to identify responses attributable to maternal obesity effects or fetal growth. We find hypoxia and induction of TNF-α signaling in syncytiotrophoblasts, while the receptor tyrosine kinases are down-regulated in cytotrophoblasts in maternal obesity irrespective of fetal growth. Notably, we identify that the fine-tune of PI3K-AKT and MAPK cascade signaling pathways in cytotrophoblasts underlies AGA versus LGA. Hofbauer cells upregulate immunometabolic genes specifically in LGA outcomes and also express most of the ligands detected only in placentas of LGA. Finally, we also use a novel microfluidic organs-on-a-chip device fabricated for co-culturing adipose spheroids and trophoblast organoids. This system recapitulates some responses of syncytiotrophoblasts to maternal obesity, offering a functionally relevant reductionistic system to study maternal-placental interaction. Our findings deconvolute key cellular and molecular adaptation of the placenta to maternal obesity and fetal overgrowth in physiological condition.

Keywords: obesity, birth weight, human placenta, single-nuclei RNA sequencing, trophoblast organoids

Main

The prevalence of obesity (BMI>30) for women at reproductive age reached 18.5% globally in 2022 and has become one of the leading concerns for their reproductive health[1]. Characterized by low-grade inflammation, hyperinsulinemia, dyslipidemia, and altered cytokines profiles, obesity adversely impacts the intrauterine environment and increases the risk of developing pregnancy-related complications[2,3]. Single-cell RNA sequencing has been performed on placentas in conditions including preeclampsia and gestational diabetes; however, the findings often reflect aggregated consequences of pathological conditions and fail to capture the multinucleated syncytiotrophoblasts (STB)[4-7]. Single-nucleus RNA sequencing (snRNA-seq) has recently provided in-depth insights into the cellular and molecular landscape of term placentas under healthy conditions[8]. Nevertheless, we still lack understanding of how the placenta adapts to maternal obesity and regulates fetal growth in the absence of severe pregnancy complications. Such insights will help identify tipping points toward pathological outcomes when compared with studies of complicated pregnancies.

The placenta is the central structure at the maternal-fetal interface, sustaining and modulating fetal growth through its metabolic, endocrine and immune functions[9]. It regulates the quantity and quality of nutrient supply from the maternal circulation by adjusting its transport capacity and nutrient uptake[10,11]. Additionally, it dynamically modulates hormonal secretion[12], and inflammation levels[13] to align with the growth requirements of the fetus. These activities are intertwined to regulate fetal development and adapt to maternal conditions[13-15]. Particularly, tumor necrosis factor-α (TNF-α) and leptin promote lipid storage in the placenta[13] and enhance the expression of amino acid and glucose transporters in trophoblast cells[16,17]. And human placental lactogen and prolactin increase maternal leptin resistance and insulin production that could in turn act on placental metabolism[14]. These activities are correlated with pre-pregnancy BMI and fetal growth[11]. Undoubtedly, the dynamic interplay between maternal conditions and the placenta serves as a potential bridge to impact fetal growth. However, our current understanding of the placental transcriptional response to maternal obesity is mostly inferred from gene expression analyses at the whole-tissue level or in primary cell cultures[18-21], which often overlook tissue complexity and the local environment. Therefore, further studies of placentas in suboptimal maternal obesity conditions are required to generate more comprehensive maps, towards an understanding of progression from physiological adaptation to pathological alteration. Here, we performed snRNA-seq on term placentas collected in a Chilean cohort study, in which women with obesity did not

develop other pregnancy complications except for more frequent birth of large-for-gestational age (LGA) infants[22]. LGA is more frequently linked to obesity during pregnancy with a prevalence of 13.41% to 38.3%[23-26], and is also recognized as a risk factor for childhood obesity, as well as metabolic, cardiovascular and neurological disorders later in life, when compared with appropriate-for-gestational age (AGA) infants[27-29].

To dissect the placental responses to maternal obesity with two different fetal growth outcomes – AGA and LGA – we subdivided the placental samples of maternal obesity by birthweight, resulting in three groups: healthy controls, maternal obesity with AGA babies (O-A), and maternal obesity with LGA babies (O-L). A Commonness-score (C-score) metric was developed to rank the extent of common and divergent transcriptional alterations in O-A and O-L compared with control. The score was applied on gene set enrichment and differential expression analysis, considering the magnitude of the alterations and the false discovery rate. The resulting pathways and genes with a high C-score were identified as common responses to maternal obesity. In contrast, those with low C-scores diverged between two obesity groups, potentially underlying the mechanisms of divergence in fetal growth. Moreover, the intercellular ligand-receptor communication network, weighted by C-scores analysis, revealed the major sources and hub cell types of these common and divergent responses. Finally, microfluidic co-culture of adipose spheroids and trophoblast organoids in a microphysiological system could recapitulate partial common responses of trophoblast cell types to maternal obesity, providing a prototype in future to study the effects of diverse maternal disease conditions on placentas in human.

Results

Cell-type annotation in placentas of three groups stratified by maternal obesity and fetal growth

In total, 22 normal-weight and 25 women with obesity were included in the cohort[22]. In addition to analyzing the response of the placenta to maternal obesity, we also aimed to investigate the interplay between the placenta and fetal overgrowth. To achieve this, we stratified samples from women with obesity into two groups: O-A (Obesity with AGA birthweight, defined between the 25th and 90th percentiles) and O-L (Obesity with LGA birth weight, defined as birthweight > 90th percentile) according to the sex-stratified weight data[30]. These two groups had no significant differences in maternal age, placental weight and placental efficiency compared with controls with AGA birthweight (Figure S1a).

We then selected 4 samples of each group with representative maternal BMI and birthweight for snRNA sequencing (Figure 1a and Figure S1a). All samples were from vaginal delivery and had comparable maternal age and placental efficiency across groups (Figure 1b). We then dissected the placental villous region and dissociated the tissue into single nuclei, followed by 10x Chromium snRNA-seq (Figure 1c). A total of 37,408 nuclei were retained for downstream analyses after stringent quality control, yielding comparable identified total counts and gene number per cell across all groups (Figure 1d). Using previously published marker genes for cell types[31], we annotated 14 placental cell types, including different trophoblasts, endothelial cells, stromal cells, and leukocytes after uniform manifold approximation and projection (UMAP) analysis for visualizing clusters (Figure 1e). There was no significant difference in the proportion of cell types, either in various trophoblast cells (Figure 1f) or in different villous non-trophoblast cells (Figure 1g), across the three groups (1).

Trophoblasts accounted for the majority of cells and were predominantly composed of syncytiotrophoblasts (STBs) and villous cytotrophoblasts (CTBs). Proliferative CTBs (pCTBs) were identified as being in the cell cycle (Figure S1b) and expressing *ATAD2*, *BRIP1* and *MKI67* in addition to other common CTB markers including *TP63, LRP5* and *CDH1* (Figure 1h). Nuclei co-expressing *ERVW-1* (Syncytin-1) and *ERVFRD-1* (Syncytin-2) were identified as early STB (eSTB), consistent with previous findings[32]. Mature STB shared

expression of *ERVW*-1 and *CYP19A1* with eSTB but also uniquely expressed *CSH1* and *PSG3* (Figure 1h). The extravillous trophoblasts (EVTs) accounted for only 0.5% of all nuclei, with fewer than one hundred per group, aligning with our villous sampling approach (Table S1). These cells were characterized by expression of *FSTL3*, *KRT7* and *PRG2* (Figure 1h). Among other villous non-trophoblast cells, stromal cells within the chorionic villi included fibroblasts and myofibroblasts. We identified fibroblasts characterized by the expression of collagen subunits (*COL3A1* and *COL1A1*) and *DCN*. Myofibroblasts were also annotated by concurrently expressing collagen (*COL3A1* and *COL1A1*), actin (*ACTA2*) and myosin (*MYH11*) subunits (Figure 1h). Vascular endothelial cells (VECs) were identified based on the expression of *CD34*, *VWF* and *CDH5* (Figure 1h). A small subset of VECs expressed arterial markers, including *EFNB2*, *GJA5*, *ARL15* and *PRDM16* (Figure 1h and Figure S1c-d) and were designated as "GJA5$^+$ VEC". The remaining VECs exhibited low expression of these markers and were named as "GJA5$^-$ VEC (Figure 1h and Figure S1c-d). Among the immune cells, we primarily captured Hofbauer cells, which are specialized macrophages located within the chorionic villi and express *PTPRC*, *LYVE1*, *F13A1* and *ITGAX* (Figure 1h). *PTPRC* was also detected in a few remaining nuclei, indicating their leukocyte origin. These cells could be further annotated into monocyte, B cells, NK cells and T cells (Figure 1h and Table S1). However, due to their very small numbers (Figure S1e), likely carried over from dissection, and being outside the scope of our study, these cells were excluded in our subsequent analyses.

Next, we focused on the major villous cell types – i.e., STB, CTB, VEC, fibroblasts and Hofbauer cells – to understand their distinct molecular signatures in the placental responses to obesity and regulation of fetal growth. To understand both transcriptional responses, as pathways and specific genes in each cell type, we developed a C-score metric to measure the transcriptional changes in the two obesity groups, O-A and O-L, compared to the control. This was done by computing both the fold-changes of differentially expressed gene (DEGs) and the false discovery rate (FDR), and then ranking the C-score from high to low. A high positive C-score indicated that genes were consistently upregulated or downregulated in both comparisons (i.e., O-A vs. control and O-L vs. control), suggesting common placental transcriptional responses to maternal obesity. In contrast, a low and/or negative C-score indicated that the two obese groups responded in opposite directions at the gene expression level when compared to controls, implying divergent regulation of the placenta associated with the fetal overgrowth outcomes (see Methods: Scoring the common or unique genes between comparisons). This method provided us with a systematic approach to study the common or divergent molecular signatures of all cell types and cell-cell communications in the placenta. The number of the common or divergent genes for each cell type are reported in Table S2.

Identification of STB subpopulations along the maturation states

The STB layer is formed through the fusion of CTBs, a process that requires remodeling of cytoskeletal and plasma membrane dynamics[32]. A total of 24,478 STB nuclei were captured, enabling us to investigate the subpopulations across the different phases of STB life cycle. We first re-clustered the STB nuclei and identified three substates (STB-a, -b and -c) (Figure 2a). To better elucidate their maturation process, we incorporated CTBs and eSTBs as early differentiation timepoints to place STBs in context for pseudo-time analysis[33] (Figure S2a). We revealed that the three STB substates were aligned along the pseudo-time axis with varying numbers of cells distributed across the timeline (Figure 2b). Novel gene markers were subsequently identified, highlighting the biological differences among the substates (Figure 2c and Figure S2b). STB-a appeared at an earlier stage characterized by the expression of *TENM3* (Figure 2c, Figure S2c), a gene encoding a teneurin transmembrane protein that promotes homophilic cellular adhesion[34]. Validation of the *TENM3*$^+$ STB-a state was previously demonstrated in the STB layer by *in situ* hybridization[35]. This state was also characterized by genes involved in cytoskeleton, tight junction, and extracellular matrix (*ITGB1*, collagen subunits *COL4A1* and *-A2*, *FN1* and *TIMP3*) (Figure 2c). Furthermore, STB-b specifically expressed *PDE4D* (phosphodiesterase 4D) (Figure 2c). Importantly, cAMP-specific phosphodiesterases, such as PDE4D, were reported to limit over-syncytialization[36]. Finally, the mature STB-c state was characterized by the expression of tight junction inhibitors such as *ADAMTS6* (a disintegrin and metalloproteinase (ADAM) with thrombospondin type 1 motif 6) and *PKIB* (cAMP-dependent protein kinase inhibitor β) (Figure 2c). The

overexpression or knockdown of *ADAMTS6* showed that it inhibited cell-cell junctions[37]. *ADAMTS6* was also identified as a marker of a STB state in a preprint study[38]. *PKIB* is involved in the cAMP pathway, which is crucial in STB formation[36]. Therefore, STB-b nuclei appeared to fine-tune syncytialization, while STB-c nuclei actively engaged in the process, collectively contributing to a dynamic balance. As excessive syncytialization leads to release of aged cytosolic material into maternal circulation[39], while restricted fusion results in exhaustion of the syncytial layer, these two subpopulations may play a critical role in maintaining STB homeostasis. Reassuringly, these STB states were further confirmed by integrating our data with a recently published term placenta snRNA-seq dataset[8] using scANVI[40] in line with previously identified various STB maturing substates (Figure S2d). These three STB states were also found across three groups, while the STB-b proportion was slightly reduced in the O-A group compared to control (Figure 2d).

Common and divergent transcriptional responses to maternal obesity among STB states

The distribution of signals across the STB layer is likely heterogeneous, and STB nuclei at different transcriptional states possibly reflect variations in functional responses to surrounding signals. Therefore, we utilized hallmark gene sets from MSigDB[41] to investigate the underlying biological pathways in maternal obesity with or without fetal overgrowth. Gene set enrichment analysis (GSEA) showed that O-A and O-L shared enrichment in the epithelial mesenchymal transition (EMT), apical junction and mitotic spindle regions only observed in STB-a nuclei (Figure S2e and Table S3). In contrast, STB-b and STB-c shared several altered pathways, including hypoxia, TNF-α signaling via NFkβ, and complement system, all of which are indicative of inflammatory processes (Figure S2e and Table S4). These signaling pathways were considered as common responses to maternal obesity in STB. We then assessed genes within these pathways using the previously described C-score metric. The score provided the most commonly (i.e., highest positive C-score) or divergently (i.e., lowest negative C-score) regulated genes between O-A and O-L groups (Figure 2e-g). In STB-a, *FN1* and *TCF7L2* were commonly decreased in both obese groups (Figure 2e), while the increase of *KISS1* was only observed in O-A (Figure 2e). In STB-b, *SEMA6A* and *GULP1* were increased in both obese groups, whereas *CSH1*, *RYBP*, and *CHSY1* were increased in O-A and lowly expressed in O-L (Figure 2f). In STB-c, *FLT1* and *PAPPA2* were increased in both obese groups, whereas *PSG4* and *PKIB* were increased in O-A (Figure 2g). The C-score also found that the elevated expression of genes driving the enrichment of the hypoxia signaling pathway in maternal obesity in STB-b and c (Figure 2h). Among them, *FOXO3* and *FOS* were reported to be at the crosstalk between hypoxia and TNF-α signaling[42-45], while *SLC2A1* (GLUT1) and *TFRC* may mediate the interaction between hypoxia and metabolism[46,47]. Specifically, GLUT1 is predominately expressed in the microvillous membrane of STB facing the maternal blood and facilitates glucose uptake from the maternal circulation[46]. Furthermore, *TFRC* contains a binding site for hypoxia-inducible factor-1 (HIF-1) within its promotor region[47]. Altogether, many of the highly ranked genes using C-score encodes for receptors and secreted proteins (Table S4), suggesting adaptation of cell-cell communication in maternal obesity regardless of fetal growth trajectories. This is in line with the function of STBs at the direct contact of the maternal conditions and could adjust the transport and hormonal expression accordingly.

Using a previously published set of placenta-specific secreted proteins[48], we found that some of the genes responsive to maternal obesity encoded these proteins, especially in STB-b (Figure 2i). Expression of *CSH1* (encoding human placental lactogen (hPL) hormone) differed between obesity groups: elevated in O-A whereas decreased in O-L (Figure 2j). In contrast, *FBN2*, a gene encoding a peptide hormone known as placensin that can upregulate glucose secretion[49], was only elevated in the O-L group (Figure 2j). Such hormone regulation could be a part of the adaptation of the placenta to maintain proper fetal growth, while its altered secretion could lead to unbalanced fetal growth. Although STB nuclei might have different functional roles at different maturation states, we still identified seven genes that respond robustly to maternal obesity at all STB nuclei states (Figure 2k). Among them, *CGA* and *GULP1* were upregulated, while *CLIC5*, *FBLN1* and *HSP90AA1* were downregulated (Figure 2k). *CGA* is of interest as it encodes the alpha unit of human glycoprotein hormones, including hCG (chorionic gonadotropin). Changes in hCG levels have previously been

linked to placental dysfunction and contribute to adverse pregnancy outcomes[50]. Moreover, of the four genes that responded differently according to fetal growth in both STB-b and STB-c, three of them encode for receptors (Figure 2l). *AHR* (aryl hydrocarbon receptor) encodes a receptor that senses the varied cellular environment, and could be activated by the endogenous tryptophan derivatives. Tryptophan is an essential amino acid critical for placental and fetal development[51]. *ANO2* (calcium-activated chloride channel anoctamin-2) encodes a Ca^{2+} sensor. *LIFR* (leukemia inhibitory factor receptor) encodes the receptor of LIF, which is essential for early implantation. In mice, LIFR deficiency led to impaired placenta differentiation and reduced embryo viability, and increased birth weight[52].

Regulation of CTBs responses by PI3K-AKT and MAPK cascade signaling pathways

Next, we analyzed the enrichment of hallmark gene sets in CTBs, the progenitors giving rise to the STB layer. In contrast to the STBs, we predominantly detected common responses, with expression of many genes being decreased in hallmark gene sets in both O-A and O-L (Table S3). These pathways included apical junction, mitotic spindle, G2M checkpoint, adipogenesis, IL2-STAT5 signaling, heme metabolism and hypoxia (Figure 3a). Interestingly, only the Myc target pathway showed a divergent response, manifested as an overall decreased expression in the O-L group (Figure 3a). We identified 102 genes as commonly dysregulated to maternal obesity. *PDE3B* (Phosphodiesterase 3B) was among the top three most dysregulated genes, along with *PLD5* and *C5orf12* (Figure 3b). *PDE3B* may play a role in the metabolic response to maternal obesity, as it was reported be regulated by hormones from the maternal circulation to influence energy homeostasis[53].

To interpret the function of the downregulated genes (i.e., 100/102) observed in two obesity groups, we investigated their biological process ontologies and found significant enrichment for the PI3K-Akt signaling pathway (Figure 3c). Specifically, genes highlighted in red are related to receptor tyrosine kinases (RTKs) in transducing the growth factor signaling (Figure 3c). It has been well characterized that *HSP90AA1* is essential for stabilizing AKT activity, which in turn facilitates the phosphorylation and inactivation of FOXO3[54]. Among divergent genes, 9 and 15 genes were upregulated in O-A and O-L, respectively (Figure 3d). Interestingly, five genes were annotated for positive regulation of MAPK cascade and were only upregulated in O-A (Fig.3d). MAPK cascade is also an intracellular signaling pathway downstream of RTK, similar to the PI3K-AKT signaling pathway. Likely, in O-A, there appeared to be counterbalanced regulation converging on FOXO3 phosphorylation (Figure 3e), which is known to be regulated by both the MAPK and PI3K signaling pathways[55]. In contrast, in O-L, there was a lack of counterbalance in FOXO3 regulation, which was also in line with decreased Myc targets (Figure 3a), as nonphosphorylated FOXO3 inhibits Myc target genes[56]. We did not find enriched functional pathways for 15 genes upregulated in O-L. But among them, *ERBB4*, encoding an EGFR, was upregulated in the O-L group and was reported to be expressed by CTB but not EVT[57] as a pro-survival factor in the CTB cell line under hypoxic conditions[58].

Common and divergent transcriptional responses in non-trophoblast cell types

VECs line the blood vessels within the villous structures, facilitating gas and nutrient exchange between the maternal and fetal circulation. In VECs, the majority of hallmark gene sets were decreased in both the O-A and O-L groups (Table S3). Common gene sets included IL2-STAT5 signaling, complement signaling, KRAS signaling, G2M checkpoint, heme metabolism, protein secretion, and adipogenesis (Figure S3a). The C-score analysis identified 33 genes with common response, including *FN1*, *COL4A2* and *NRP1*, while only three genes (*GRK5*, *CALCRL*, and *FCGR2A)* were divergently regulated (Figure 4a). Five common response genes (*NRP1*, *GNA14*, *COL4A2*, *COBLL1*, and *RAPGEF5)* have been reported among 299 genes co-expressed with *FLT1* (VEGF-R1)[59] (Figure 4b). Genes encoding the VEGFA complex[60] were downregulated in both O-L and O-A (Figure 4c). VEGF-A complex binding to VEGF-R1 increases angiogenesis[61], hematopoiesis[62], and inflammatory cell recruitment[63]. *FN1* (Fibronectin) has been shown to regulate VEGF-A expression[64], cellular apoptosis, and autophagy[65] in human umbilical vein endothelial cells. In addition, *NRP1* (neuropilin-1) is an

adaptor protein forming dimers with VEGF-A or Sema3 to bind VEGFR[66]. Our findings suggest that the angiogenesis processes, involved in VECs, may be particularly dysregulated by maternal obesity.

Hofbauer cells are specialized macrophage-like cells within the placental villi. In Hofbauer cells, the G2/M checkpoint signaling pathway, which regulates cell proliferation, was found to be suppressed in both groups of maternal obesity (Figure S3b). The PI3K-AKT-mTOR signaling pathway, a key regulator of nutrient-sensing and tissue growth, was also suppressed (Figure S3b). Another key function of Hofbauer cells is cytokine secretion[67], which was reduced in both the O-A and O-L groups (Figure S3b). The C-score analysis identified 30 common response genes in maternal obesity, including the downregulation of *CTSC* (Figure 4d). *CTSC*, encoding the lysosomal cysteine protease Cathepsin C, plays an important role in immune system regulation and macrophage activation[68]. The inflammatory response, together with TNF-α signaling mediated by NFKβ, IL-STAT5 and hypoxia pathways, was divergently regulated in placentas of O-A and O-L (Figure S3b). These signaling pathways were decreased in the O-A group, whereas increased in the O-L group (Figure S3b). The genes assigned with significantly low C-scores might drive these divergent hallmark pathways (Figure 4d). Among these genes involved in inflammatory response (Figure 4e), *FKBP5* encodes for a protein from the immunophilin protein family that may promote NFKβ-mediated inflammation[69]. *NAMPT*, also known as Visfatin or PBEF, has a dual role as an enzyme regulating glucose homeostasis and as a cytokine, particularly expressed in the fetal membrane[70]. *SRGN*, on the other hand, encodes a major secreted proteoglycan in macrophages and promotes TNF-α secretion upon lipopolysaccharide stimulation[71]. Of note, *SLC1A3*, encoding a glutamate transporter, was increased only in the O-L group and its ontologies include NF-κB, IL/STAT5, and mTORC1 signaling. In contrast, *ADAMTS2*, an anti-inflammatory metalloproteinase[72], was only increased in the O-A group. These findings highlight potential molecular mechanisms contributing to an elevated inflammatory response in Hofbauer cells, observed only in maternal obesity associated with fetal overgrowth.

Next, we aimed to understand how fibroblasts respond to maternal obesity. Fibroblasts are essential components of the stromal compartment of the villous core, playing multifunctional roles critical for villi architecture, vascular development, immune regulation, and support of trophoblast functions[73]. In fibroblasts, GSEA hallmark gene sets, including KRAS signaling, PI3K-AKT-mTOR signaling, adipogenesis and apoptosis, were commonly suppressed in both O-A and O-L conditions (Figure S3d). However, the suppression of TNF-α signaling via NFKβ was only seen in the O-A group, while this signaling was elevated in the placentas of the O-L group (Figure S3d). C-score analysis further identified genes enriched in these pathways, among which common response genes included *GNA14*, *PTPRT* and *PTPRD* and divergent response genes were *IRS2*, *PID1*, *SERPINE1*, *FOXO1*, *PDK4* (Figure 4f-g). In addition, six common genes were annotated as GEFs (Guanine nucleotide exchange factor), regulators of GTPase activity. These GTPase regulators control multiple small GTPases that are involved in the feedback loop culminating in PI3K activation[74] and their expression was decreased in both O-A and O-L (Figure S3e). Downregulation of GTPase regulators and activation of PI3K-Akt pathway were observed in both groups with maternal obesity (Figure S3 d-e).

The genes that were divergently altered between O-A and O-L were predominantly enriched in gene sets related to fatty acid response, insulin receptor signaling and transmembrane RTK signaling. The expression of genes such as *PID1* (phosphotyrosine interacting domain-containing protein 1), *PDK4*, *FOXO1* and *IRS2* (insulin receptor substrate 2) was significantly elevated particularly in the O-L group (Figure 4g). The increased *FOXO1* transcription activity in the nucleus leads to the expression of target genes like *PDK4* and phosphorylation of FOXO1 via IRS-2, and the PI3K-Akt mTOR signaling pathway promotes its translocation from the nucleus to the cytoplasm[75]. In summary, although the GTPase and PI3K-Akt signaling pathways - typically phosphorylating and inactivating FOXO1 - were suppressed in maternal obesity groups, FOXO1 transcript levels were notably elevated in cases of fetal overgrowth (Figure 4h). In the O-L group, fibroblasts may exhibit elevated FOXO1 transcription factor activity, which could be linked to TNF-α induced apoptosis[76].

Cell-cell communication regulated by common and divergent responses in the placenta

Our analyses have so far dissected the transcriptional response of major placental cell types in response to maternal obesity or fetal growth outcomes. However, we still did not understand whether and how these cell types communicate with each other, and coordinate either common or divergent responses within the placenta. Therefore, we utilized the consensus resources including "CellPhoneDB", "CellChatDB", "ICELLNET", "connectomeDB2020", and "CellTalkDB" from Liana+[77] to understand the ligand-receptor interactions between cell types within villi. To identify ligands expressed by each cell type that mediate signaling to other cell types, we first constructed a weighted directional regulation network, which mapped cell type-ligand to cell type-receptor (Extended Data Fig 4a). To reveal the biological relevance of these interactions, we weighted the edges of ligand-receptor pairs with average C-scores of gene pairs encoding ligands and receptors and used these values as weights and p-values, based on the genes encoding them. The ligand-receptor network was separately analyzed into ligand-receptor pairs in common responses to maternal obesity or in divergent responses related to fetal overgrowth. All ligand-receptor pairs, between each cell type pair, were summarized to provide an overview of the ligand-receptor regulation in the context of common responses to obesity (Figure 5a) and divergent responses related to fetal overgrowth (Figure 5b). We then performed centrality analyses for each cell type based on ligand expression to identify the important cell types and most-regulated ligand-receptor pairs in both contexts. At the cell type level, a high out-degree centrality (i.e. the size of the circle of each cell type) indicates the cell type that plays a major role in regulating ligand expression. A high betweenness centrality indicates the cell type that frequently acts as a "hub", interacting with multiple cell types by sending and receiving signals. While a high in-degree centrality indicates the cell type that regulates receptors in response to ligands, observed in maternal obesity groups.

Our analysis revealed that VECs had the highest out-degree centrality in common responses (Figure 5a), suggesting that VECs were highly responsive to maternal conditions and likely represented an important source of ligand signaling to regulate other placental cell types (Figure 5a). In the divergent response related to fetal growth, Hofbauer cells showed the highest out-degree (Figure 5b). Specifically, *FN1* upregulated in VECs showed highest out-degree in the common response network, suggesting increased *FN1*-receptors interaction with other cell types (Figure 5c). In the divergent response network, *SPP1* (OPN) that was expressed in Hofbauer cells, was highly associated to divergent response receptors on other cell types (Figure 5c). Next, the betweenness centrality was calculated to identify the "hub" cell type in either the common or divergent response network by sending and receiving signals. We identified that STB-c played the crucial role in most common responses by relaying signaling among other cell types, while fibroblasts were central to the most divergent responses, also by mediating signaling among other cell types (Figure 5d). We then analyzed in-degree scores across cell types, representing the reception of signaling based on receptor expression. STB-c emerged as the primary signaling target, followed by CTBs in common responses (Figure 5e). In divergent responses, fibroblasts also exhibited the highest in-degree levels, although the differences across cell types were relatively small (Figure 5e). The gene expression patterns confirmed this network analysis. Specifically, ITGA3_ITGB1 receptor complex was upregulated in STB-c shown highest in-degree, suggesting increased ligand-ITGA3_ITGB1 interaction with other cell types (Figure 5f). In the divergent responses, related to fetal growth, DSCAM showed the lowest in-degree in fibroblasts (Figure 5f). Furthermore, we highlighted several key ligand-receptor pairs identified in these analyses, which underpinned cell-cell communications in both common and divergent transcriptional responses. The highly regulated ligand-receptor pairs in common responses observed between VEC and STB-c were VEGFC- FLT1, FN1 -ITGAV and ITGB3, FN1-FLT4, as well as BMP6-BMPR2 (Figure 5g). For the interaction observed between STB-c and CTB, the growth-promoting signaling pairs like CSHL1-GHR/PRLR, LAMA3-ITGB4, SEMA6A-PLXNA2 and ANXA1/TGFB1-EGFR were noted with high C-scores (Figure 5g). *CSHL1* encodes a human placental lactogen, that can bind to the growth hormone receptor consisting of GHR and/or PRLR dimers. Additionally, epidermal growth factor (EGF) is required for proper control of growth and differentiation of CTB into STBs[78], and altered EGFR expression has been associated with placental pathologies, including intrauterine growth restriction[79]. Interestingly, receptors for these growth-promoting ligands were found decreased in CTBs, suggesting active adaptation to maternal obesity. Key ligand-receptor pairs identified underlying cell-cell

communications in divergent transcriptional responses were observed between Hofbauer and fibroblast cells, with ligand-receptor pairs SPP1-ITGB1 and TIMP2-CD44 (Figure 5h). *SPP1*, previously shown to be upregulated in macrophages within the adipose tissue during obesity[80], and bind to integrin receptors, such as *ITGB1*, which are expressed in fibroblasts of the O-L group (Figure 5h). In contrast, *TIMP2* was upregulated in Hofbauer cells of the O-A group (Figure 5h). *TIMP2* encodes a tissue inhibitor of metalloproteinases and forms a multiprotein complex with CD44 at the cell surface, which influences tissue remodeling[81]. SPP1-CD44 signaling, enhances the activation of PI3K signaling, along with the upregulation of IRS2 and FOXO1, and supports an increased PI3K pathway in the O-L group (Figure 4g-h).

Modeling the obese uterine milieu with a microfluidic co-culture of primary human adipose spheroids and trophoblast organoids

Finally, we sought to understand whether any of the observed transcriptional changes in the placenta could be attributed to organ-organ communication. Here, we particularly investigate the influences of adipocytes on the placenta trophoblast cells, using a microfluidic co-culture system of human term placenta-derived trophoblast organoids (TOs) and primary adipose spheroids (ASs). The microfluidic device[82] were were fabricated using micro-reaction injection molding (μRIM) of off-stoichiometric thiol–ene–epoxy (OSTE+). The device was then sealed and assembled using other polymer parts including Poly (methyl methacrylate) (PMMA) and Polydimethylsiloxane (PDMS). The main component of the fluidic device contains three sets of interconnected tissue chambers, arranged in pairs, enabling parallel perfusion for triplicate experiments. To ensure gas permeability and conformal contact, a PDMS layer—never in direct contact with the culture media—was applied over the fluidic layer, and finally, an additional layer of PMMA was mounted on the top. It provided a stable chip-to-world connection and ensured sealed perfusion when inlet and outlet connectors are assembled (Figure 6a). The medium was optimized for glucose, insulin and free fatty acids to simulate an obese physiological condition, consistent with its prior use for ASs culture[83]. In the first chamber pair of the microfluidic chip, we placed ASs grown in such "obese" conditions, with medium flowing towards the TOs (Figure 6a). The second chamber pair was designated for a medium control condition, without ASs. The TOs and ASs were grown and matured separately according to well-established protocols[83,84] before seeded into the device. The ASs were established from white adipose tissue of female origin and cultured for a total of 17 days in "obese" conditions before introduced in the microfluidic device. ASs displayed large lipid droplets stained by BODIPY, consistent with previous findings[83] (Figure 6b). TOs were embedded in Matrigel and supplemented with a rich medium to promote its stemness and growth[85]. TOs exhibited a typical inverted morphology as shown due to Matrigel embedding[85], with CTBs forming the outer layer shown by E-cadherin staining, and STBs embedded inside the inner layers shown by CGβ staining (Figure 6b).

We thereafter performed Prime-seq bulk RNA sequencing on TOs, comparing those from the co-culture with AS to those cultured in medium control condition, followed by the differentially expressed gene (DEGs) analysis. After the continuous exposure to obese ASs, TOs exhibited upregulation of genes related to trophoblast development, including *LEP*, *IGF2*, *PPARG*, *ASCL2*, together with angiogenesis regulators such as *FLT1* and *PGF* (Figure 6c). Metallothionein-encoding genes *MT1A*, *MT1E*, *MT1X*, and *MT2A* were significantly downregulated (Figure 6c). To determine whether the co-culture model could recapitulate certain effects of maternal obesity on the placenta, we compared the resulted DEGs of TOs with either common or divergent response genes of all cell types from snRNA-seq of placentas. Notably, 26 of 27 overlapping genes were identified in both TOs and STBs, with only one gene in common with other trophoblasts cell types (Fig 6d). Among them, genes encoding placenta-specific secreted proteins[48], *CGA*, *PSG3*, *PSG11*, *CSH2*, and *TFPI2* were upregulated (Figure 6e). *LGALS14*, important for membrane integrity, was also upregulated (Figure 6e). More importantly, 23 DEGs were highly expressed in TOs co-cultured with AS in "obese conditions", suggesting directly influenced by secretions from AS. Interestingly, there lacked overlaps between TO DEGs with the divergent response genes related to fetal overgrowth in trophoblasts. This suggests that placental-fetal interactions likely underpin the divergent responses, a complexity that our microfluidic co-culture system is unable to capture, as it focuses solely on placental responses to maternal conditions.

Discussion

How the human placenta regulates nutrient supply under various maternal physiological conditions to meet fetal growth requirements remains an intriguing question. In this study, we examine the placentas of women with obesity who delivered infants of varying birth weights to understand the physiological adaptations to maternal uterine environments and their relationship to different fetal birth outcomes. Given that the human placenta is a highly specialized organ with distinct cell types, including the multinucleated STB layer, we utilized snRNA-seq. Our study revealed cell-type-specific transcriptional responses to maternal obesity, including common responses across cell types and divergent responses associated with varying birth weights. We highlighted that cell-cell communication among the cell types could play a key role in mediating these common and divergent responses. All these findings are summarized in Figure 7.

Previous studies suggest that maternal obesity alters metabolites, hormones and cytokines[86-90] such as IL-6 and TNF-α, which can be sensed by trophoblast cells[91] and thus influence trophoblast proliferation[92], nutrient uptake and transport[16,93]. Further, activation of phospholipase A2 by TNF-α and leptin, in human trophoblast cells, has been proposed as a mechanism that promotes excessive fetal fat accumulation and neonatal adiposity[90]. Our findings show that STBs in the human placenta exhibit elevated hypoxia and TNF-α signaling via NFKβ under conditions of maternal obesity. These responses were potentially driven by *FOS* and *FOXO1*, and *SLC2A1*. *SLC2A1* encodes GLUT1 (glucose transferase 1) which promotes glucose uptake. This suggests that, as in other metabolic organs, there is an interplay between hypoxia, inflammation and excessive nutrient transport present specifically in the STBs. CTBs respond to maternal obesity by downregulating gene expression of genes involved in PI3K-Akt signaling pathways, particularly those associated with the *GHR* (growth hormone receptor), *PRLR* (prolactin receptor), and *CSF3R* (Colony Stimulating Factor 3 Receptor). It is likely that CTBs actively adapt via these receptors to the ligands expressed by STBs, as well as those diffusing from the maternal circulation through the STB layer. Using a systematic approach to analyze ligand-receptor interactions between cell types within placental villi, we found that mature STBs (i.e. STB-c) control most of the ligand signals in maternal obesity. They expressed higher levels of growth-promoting ligands that could bind to receptors in CTBs. Although our sample profiling did not include the decidua, we observed altered growth factors receptors binding to insulin-like growth factor, prolactin, and colony-stimulating factors, which are reported to be particularly elevated in obese circulations[94,95]. These factors, derived from maternal or possibly fetal sources, could pose effects on promoting tissue growth, including fetal overgrowth, if they are not properly regulated in CTBs.

Moreover, we identified expression patterns associated with fetal overgrowth in maternal obesity, referred to as divergent responses. Notably, TNF-α signaling and inflammatory response were decreased in the Hofbauer cells of the O-A group, whereas they were increased in the O-L group. Genes that play a dual role in inflammatory response and metabolism, such as *NAMPT*[96] and *GLUT3*[97], were only upregulated in the O-L group. Their expression might facilitate the immunometabolic modulation by Hofbauer cells related to fetal overgrowth. Ligand-receptor network analysis revealed that Hofbauer cells were the primary ligand senders in divergent responses. Hofbauer cells over-expressed the ligand *SPP1* in the O-L group. In a hypoxic environment, as often found in tumors, macrophages can adopt a specific polarized phenotype characterized by the upregulation of *SPP1*[98]. This polarization supports tumor progression by promoting cell survival, angiogenesis, and immunosuppression. Previous studies reported that dysregulated Hofbauer polarization and immune regulation can also restrict fetal growth[99-101]. While the role of the placenta as an immunomodulator remains poorly understood, our study suggests that the characteristic gene expression of immunomodulatory Hofbauer cells is related to the fetal overgrowth in women with obesity.

Notably, an increase in transcriptional activities involving TNF-α signaling in fibroblasts was observed only in the O-L group. TNF-α signaling may impair insulin action on fibroblasts by inhibiting the activation of IGF-1/insulin hybrid receptors[102]. In fibroblasts, the increase of both TNF-α signaling and genes involved in insulin receptor signaling, such as *IRS2*, exclusively in the O-L group, suggests that these regulatory mechanisms may contribute to fetal growth. Fibroblasts were also the major information “hub” relaying signals associated with

fetal overgrowth. It has been suggested that the most expressed ligand for fibroblasts is macrophage-derived *SPP1*, which has been shown to activate myofibroblasts in fibrosis[103]. While fibroblasts and stromal cells in the term placenta have been understudied or even overlooked in prior research, our analysis sheds light on their transcriptional responses to maternal obesity, particularly under conditions of fetal overgrowth. Furthermore, TNF-α signaling was increased in the STBs of both obesity groups, while only increased in Hofbauer cells and fibroblasts in fetal overgrowth. This may indicate that the STB layer response to TNF-α is predominantly shaped by direct exposure to maternal inflammatory signals. However, within the placental villi, these maternal signals are likely to be balanced, to achieve appropriate fetal growth. This regulatory mechanism might be critical to protect the placental environment from excessive inflammatory responses. If these cell types efficiently reduce inflammatory signaling, the fetus of a mother with obesity could still have an appropriate birth weight. Conversely, an inadequate response may increase the inflammatory response and contribute to excessive fetal growth.

When investigating the intercellular communication network in the inter-villous cell-to-cell communication, we found that STBs had the highest contribution to the overall ligand-receptor pairs observed in common transcriptional responses. Therefore, the STBs were considered as the primary 'hub' for the integration of signals relevant to maternal obesity, but irrelevant to fetal growth. Whether the signals originate from maternal circulation or villous cells cannot be concluded from the snRNA-seq data. However, using our organoid co-culture system, we were able to infer that some signals were likely derived outside the villi. The unidirectional media flow from the ASs to the TOs demonstrated the response of the trophoblasts to the potential metabolites and cytokines from the obese maternal circulation. The STBs exhibited a greater overlap of common response genes to maternal obesity with DEGs in TOs compared to any other cell type. This response is significant considering that the STBs are located within the TOs and not on their surface. The increased expression of secreted proteins, as well as *FLT1* and *PPARG* which are associated with vascular endothelial proliferation-associated, could be due to factors released from adipose tissue during maternal obesity. However, we are aware that the expression changes related to fetal overgrowth have not been validated with such system. Due to technical and ethical constraints, later-stage embryonic models can only represent specific aspects of fetal development, but not overall growth[104]. Nevertheless, our results support that immunometabolic modulation of Hofbauer cells is at the center of such responses and provides the potential targets that can be tested in animal models and/or human embryo models, provided that these models are evaluated as valid and representative.

In conclusion, our analysis of the common and divergent signaling pathways and genes that respond to maternal obesity and fetal growth provides a deeper understanding of the molecular mechanisms underlying physiological adaptation to maternal obesity. This study suggests a finely regulated response involving hypoxia, nutrient transport, inflammation, and TNF-α signaling, all of which are influenced by maternal conditions and fetal growth signals. Identifying specific cell types and molecular alterations that contribute to fetal overgrowth may assist with personalized care during pregnancy and future risk assessment for adverse health outcomes in offspring. As obesity is expected to continue to increase, this knowledge is crucial for the development of future intervention strategies.

Figures

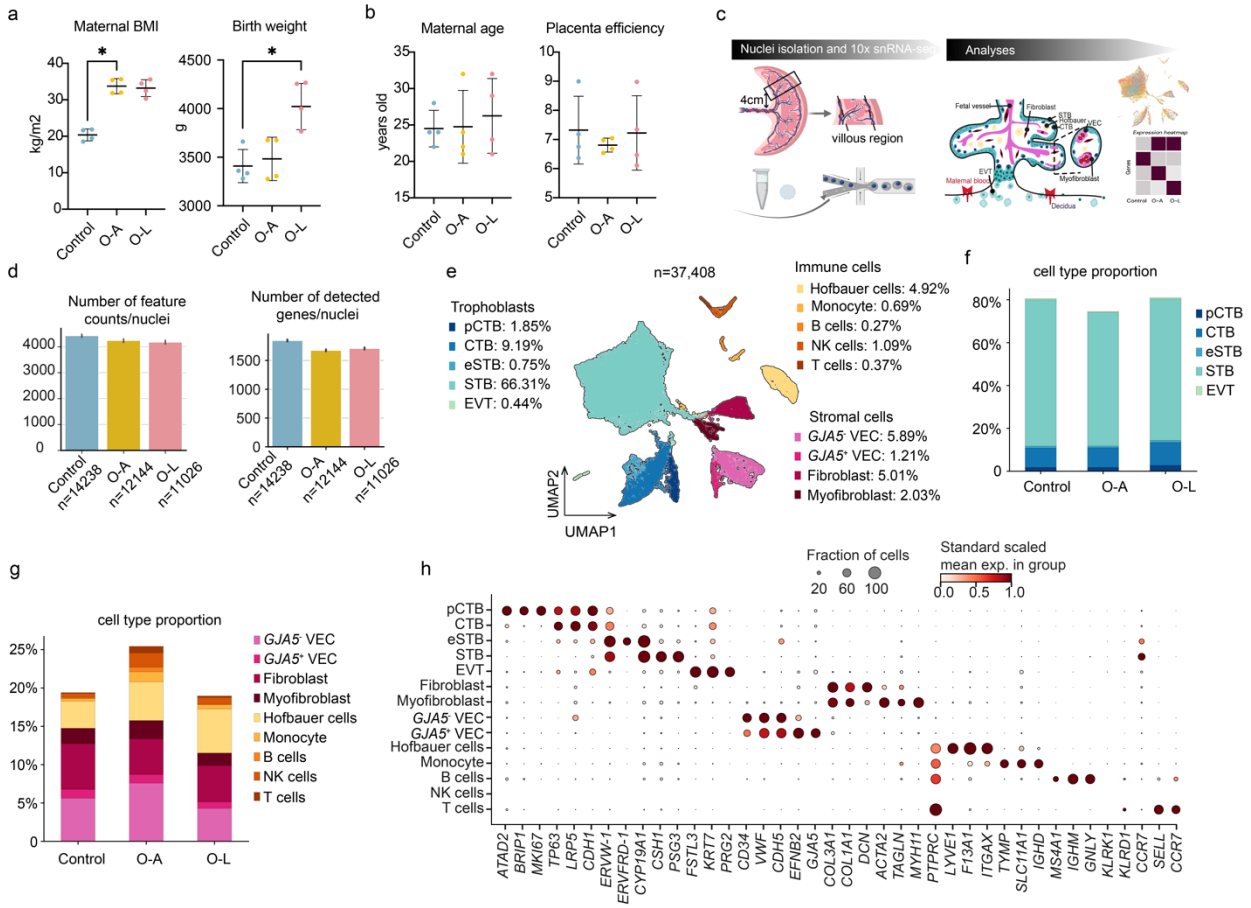

Figure 1 snRNA-seq of the human placentas from normal-weight mothers and mothers with obesity stratified by fetal birthweight. a-b, Maternal BMI (body mass index), and birthweight of samples for snRNA-seq from each group (x-axis). **b,** Maternal age, and placental efficiency of samples for snRNA-seq from each group (x-axis). **c,** Experimental procedures. **d,** Number of total count per nuclei and nuber of detected genes per nuclei. **e.** Two-dimensional UMAP (Uniform manifold approximation and projection) of 37,408 nuclei profiles (dots) from all donors (n=12), colored by cell type. **h,** Mean expression (dot color, gene standard scaled across all cells of a type) and fraction of expressing nuclei (dot size) of marker genes (columns) for each of the 14 major cell types (rows). **f,** Stacked barplot showing trophoblast cell proportion in each group. **g,** Stacked barplot showing showing the non-trophoblast cell types. Controls: normal-weighted women (n=4); O-A: Obese mother with appropriate for gestational age baby (birthweight within the 25th and 90th percentile of WHO growth curves); O-L: Obese mother with large for gestational age baby (birthweight >90th percentile of WHO growth curves); CTB: cytotrophoblasts; VEC: vascular endothelial cells; EVT: extravillous trophoblasts; pCTB: proliferative CTB; STB: syncytiotrophoblasts; eSTB: early syncytiotrophoblasts.

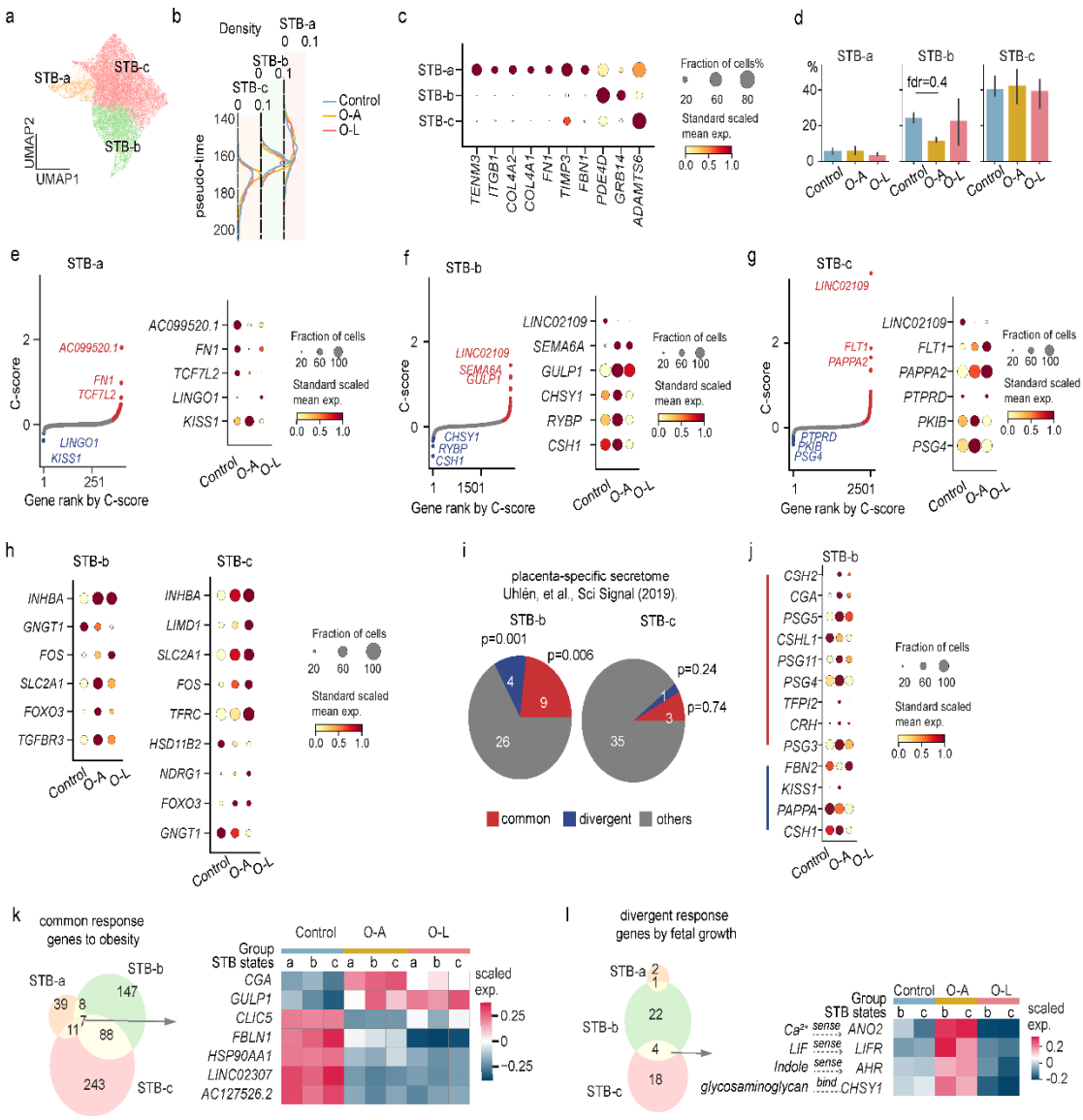

Figure 2 STB nuclei adapt to maternal obesity by adjusting the expression activities of hypoxia and transport relevant pathways. a, UMAP representation of STB colored by STB states. **b,** Pseudotime value visualization across trophoblast cell types and states. Density plot of pseudotime value colored by each group. **c,** Dotplot of genes specifically expressed in STB-a, -b or -c state. Dot color indicates the standard-scaled mean expression level of the gene. **d,** Proportion of STB states across groups. Bar height represents the mean and the error bar represents 50% interval. Data were compared by a Bayesian model[9]. **e-g,** Left, scatterplots of genes ordered by C-scores in STB-a (**e**), STB-b (**f**), STB-c (**g**). Right, dot plots showing expression of genes (y-axis) for groups (x-axis) in STB-a (**e**), STB-b (**f**), and STB-c (**g**).**h,** Dot plots showing expression of genes involved in hypoxia in STB-b (left) and STB-c (right). **i,** The proportion of common, divergent or neither common nor divergent response genes among the placenta-specific secretome reported in human protein atlas[48]. **j,** Dot plots showing expression of 13 genes shown in in STB-b (i, left pie plot). **k,** Venn plots of the common response genes in STB-a, STB-b, and STB-c (left) and a heatmap showing the gene expression of the 7 overlapping common response genes in all three states (right). **l,** venn plot of divergent response genes by fetal growth (top) in STB-a, STB-b, and STB-c and heatmap showing the expression of the divergent response genes by fetal growth in STB-b and STB-c (down). The expression is normalized, log-transformed and z-scaled in each cell state.

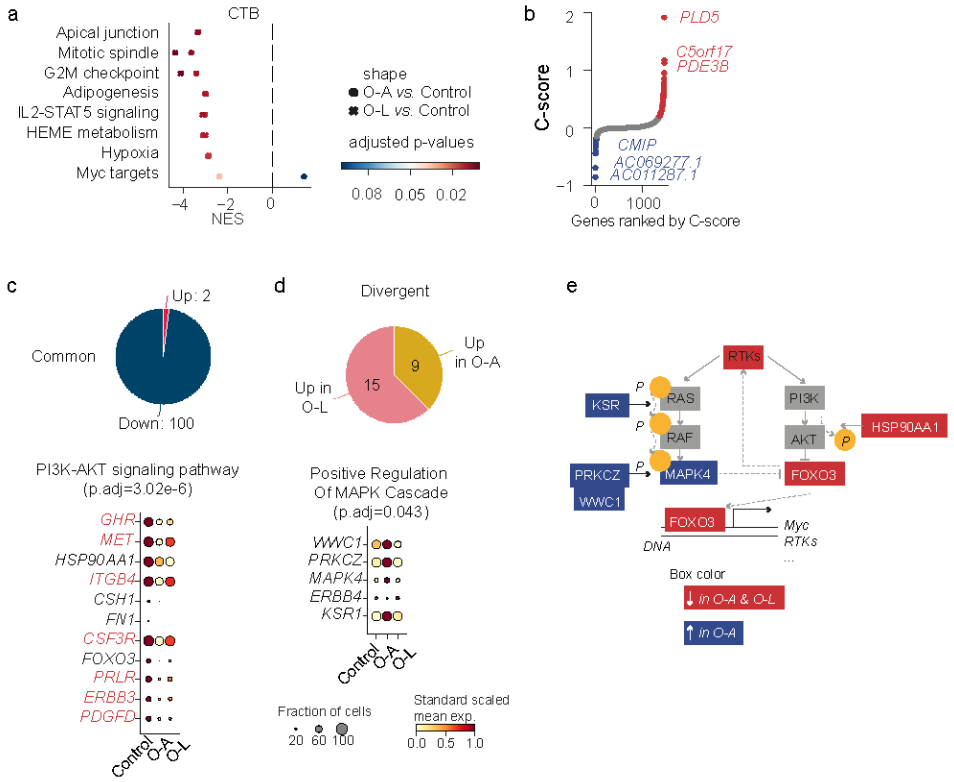

Figure 3 Alterations of gene expressions in PI3K-Akt pathway and MAPK cascade in CTBs from mothers with obesity with or without fetal overgrowth. a, Gene set enrichment analysis[10] with the enrichment score of hallmark gene sets for O-A *vs* Control (dot) and O-L *vs* Control (cross). The shapes were colored by the Benjamini-Hochberg adjusted p-values. **b,** Scatterplots of genes ordered by C-scores in CTB. **c,** Proportion of up- or down-regulated genes among the common response genes (up panel). And dotplot showing the expression of the genes involved in PI3K-Akt signaling pathway (down panel). **d,** divergently response genes (up panel) that were up-regulated or down-regulated in the mothers with obesity (O-A and/or O-L) compared with normal-weight controls (Control). And dotplot showing genes involved in the positive regulation of MAPK cascade (down panel). **e,** A summary of the response genes in PI3K-Akt pathway and MAPK pathway under the receptor tyrosin kinase signaling. The PI3K-Akt signaling was commonly reduced in CTBs from obesity groups, while the MAPK signaling was up-regulated in the obesity with appropriate birth weight group, likely to compensate for the decreased receptors and signals transducted in.

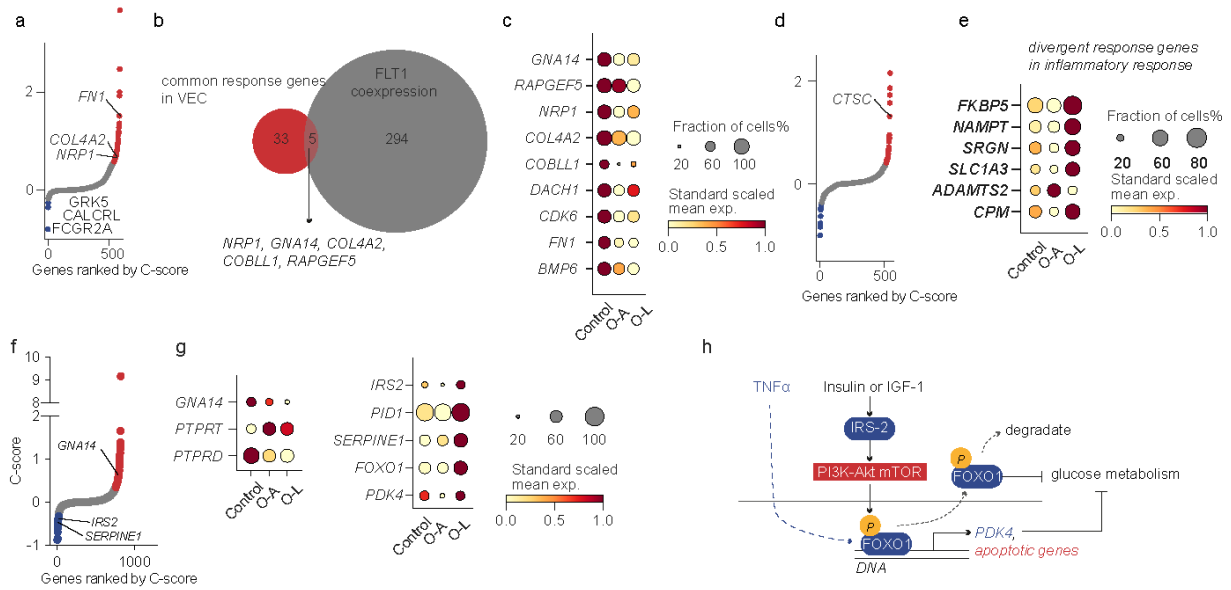

Figure 4 Alterations of gene expressions in vasculaer endothelial cells, Hofbauer cells and fibroblast from placentas of mothers with obesity with or without fetal overgrowth. a, Scatterplots of genes ordered by C-scores in GJA5- vascular endothelial cells. **b,** Overlap of the common response genes in GJA- VEC and the FLT1 co-expression genes[59]. **c,** Dotplot showing expression of genes relevant to FLT1 (VEGFR1). **d,** Scatterplots of genes ordered by C-scores in Hofbauer cells. **e,** Dotplot showing expression of genes involved in inflammatory response in Hofbauer cells. **f,** Scatterplots of genes ordered by C-scores in fibroblast. **g,** Dotplot showing expression of common (left) and divergent response genes involved in PI3K-Akt pathways in fibroblast. **h,** Illustration summarizing the pathways altered in fibroblast in obesity groups.

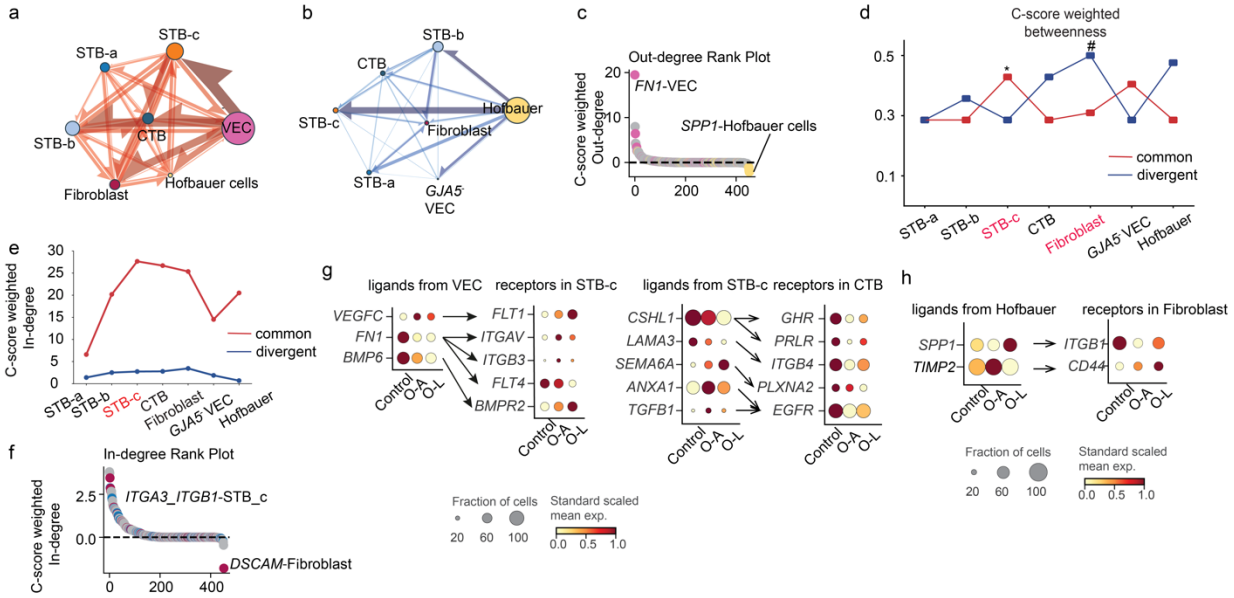

Figure 5 Common and divergent response networks of mothers with obesity with or without fetal overgrowth. a-b, Connectome ring plots for cell-cell communication build from commonly (a), or divergently (b) response ligands and among major cell types in placental villi from mothers with obesity. Different colors represent different cell types, the edge thickness is proportional to the communication strength, and edge direction goes from the sender cell type to the receiver cell type. **c,** Out-degree analysis to indicate the major common or divergent sender cells of ligands. The pink dot represents the vascular endothelial cells, and the yellow dot represents the Hofbauer cells. **d,** Betweenness centrality analysis to indicate the bridging cell types as the mediators of communication in the common response network. The * marks the most bridging cell type of the common response network while # marks the most bridging cell type of the divergent response network. e, the in-degree at the cell type-receptor level (top) and aggregated cell type level (bottom). **e,** In-degree centrality analysis to indicate the bridging cell types as the mediators of communication in the common response network. **f,** In-degree centrality analysis at the celltype-ligand level. **h,** The dot plot of the expressions of the ligands from the STB-c the receptors from CTB (left), and the ligands from the VEC to receptors from STB-c (right). **g,** The dot plot of the expressions of the ligands from the most divergent response sender (Hofbauer cells) and the receptors from the most bridging cell type (fibroblast).

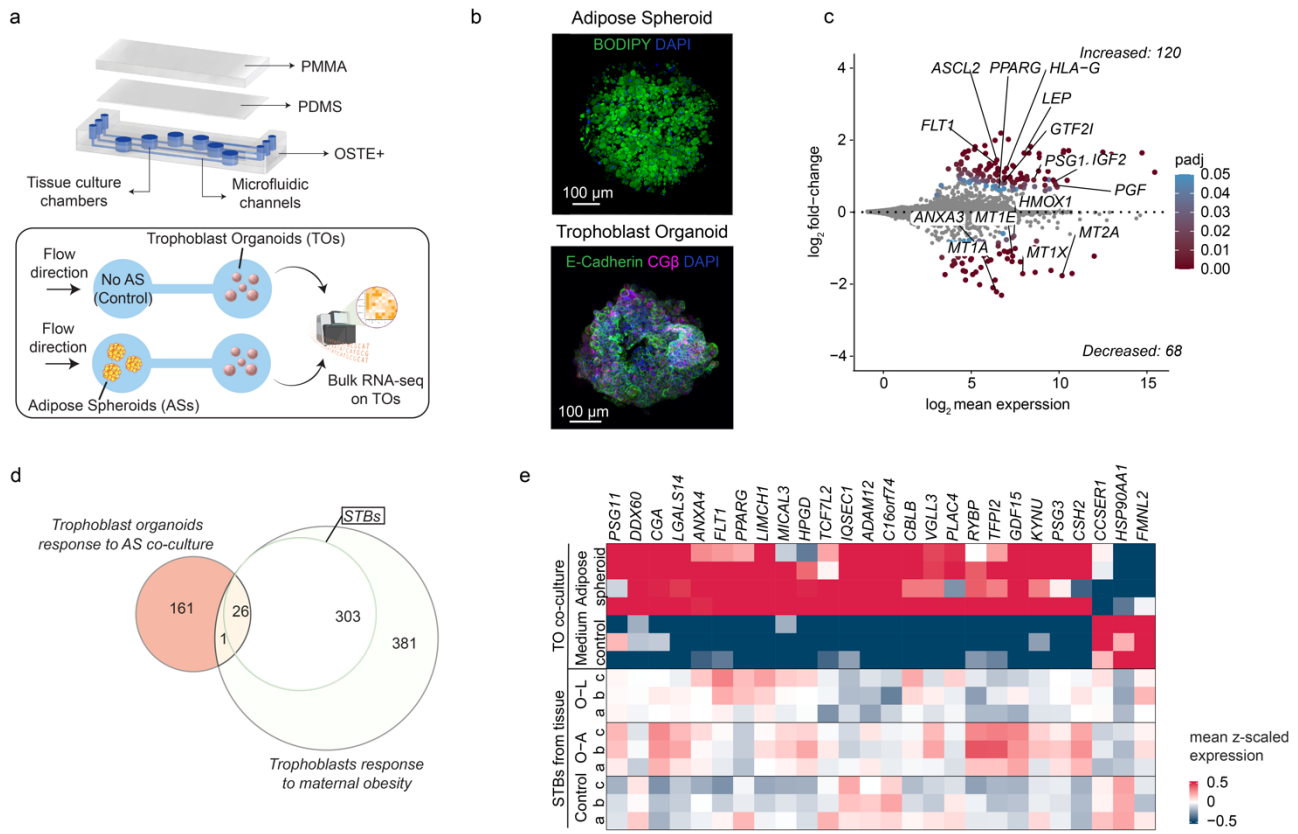

Figure 6 Trophoblast organoids continuously co-cultured with adipose spheroids replicated the transcriptional response observed in the syncytiotrophoblasts of the mothers with obesity. a, design of the microfluid device and co-culture experiment of TOs (trophoblast organoids) and AS (adipose spheroids). **b,** Representative images of ASs (up; stained with BODIPY and DAPI to highlight neutral lipids and nuclei, respectively) and TOs (bottom; stained with E-cadherin, CGβ and DAPI to highlight CTBs, STBs and nuclei, respectively). Images were captured with 10x magnification. **c,** MA plot of the gene expression of the TOs co-cultured with ASs compared with TO cultured solely on the microfluidic platform. **d,** Venn diagram showing the overlap of the differentially expressed genes in the microfluidic co-culture experiment and trophoblast response to maternal obesity. **e,** expression heatmap for the 26 overlap genes in (d).

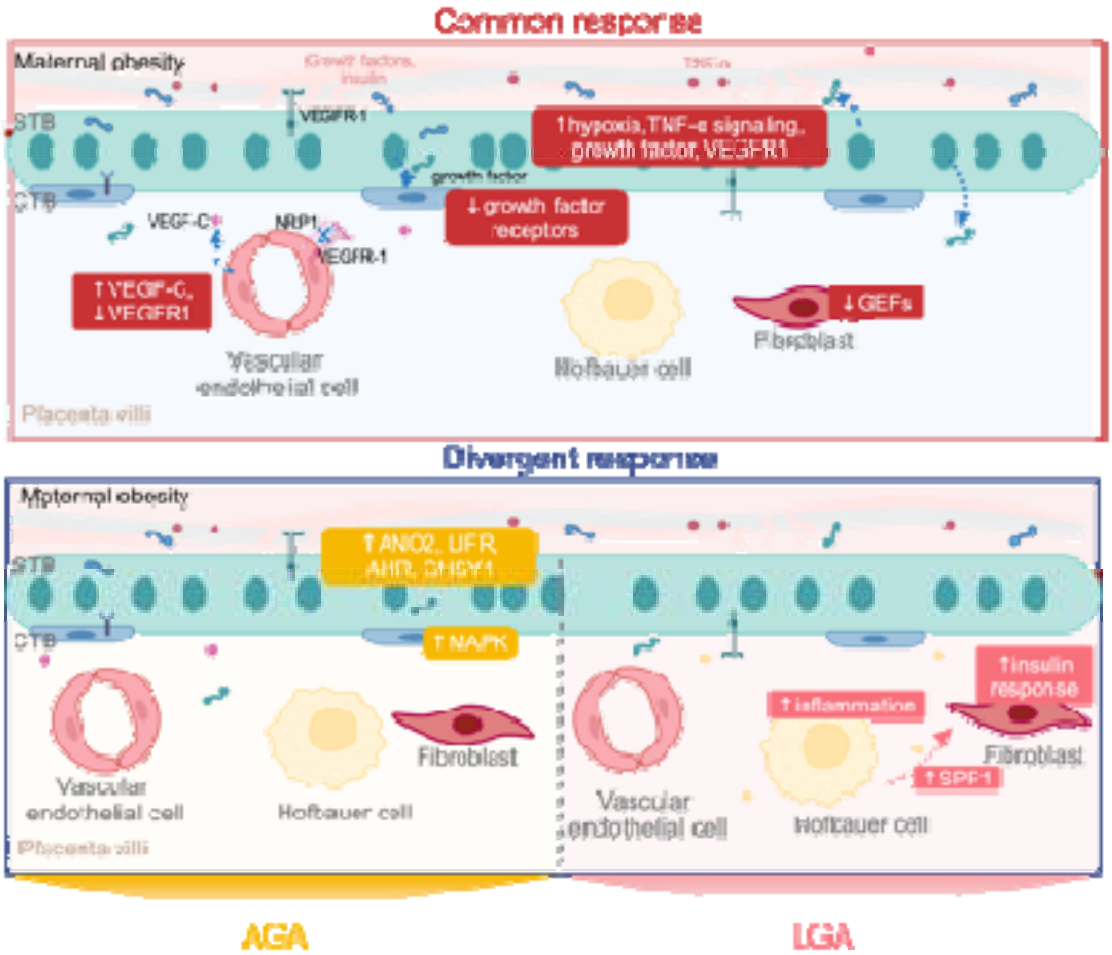

Figure 7 Schematic summary of the present work, showing that gene expression responses to maternal obesity, commonly observed in obesity groups (up-panel). And the gene expression changes that adapt to appropriate or large birth weight (bottom-panel). The dashed box includes the implied cellular function, where an increase of hypoxia and endocrinal growth factors in syncytiotrophoblasts confronting an obese maternal environment, and a decrease of growth factor receptors on CTBs (cytotrophoblasts) and vascular endothelial cells. Moreover, the intra-villous cell types adapt to these changes by either to balance the cellular proliferation and tissue-growth by the feedback counteracting the decreased growth factor receptors with elevated MAPK signaling in CTBs in the appropriate birth weight group. While such feedback is not activated in large birth weight group. They instead elevated the tissue-growth signaling in fibroblast and inflammatory response in Hofbauer cells.

Supplementary Material

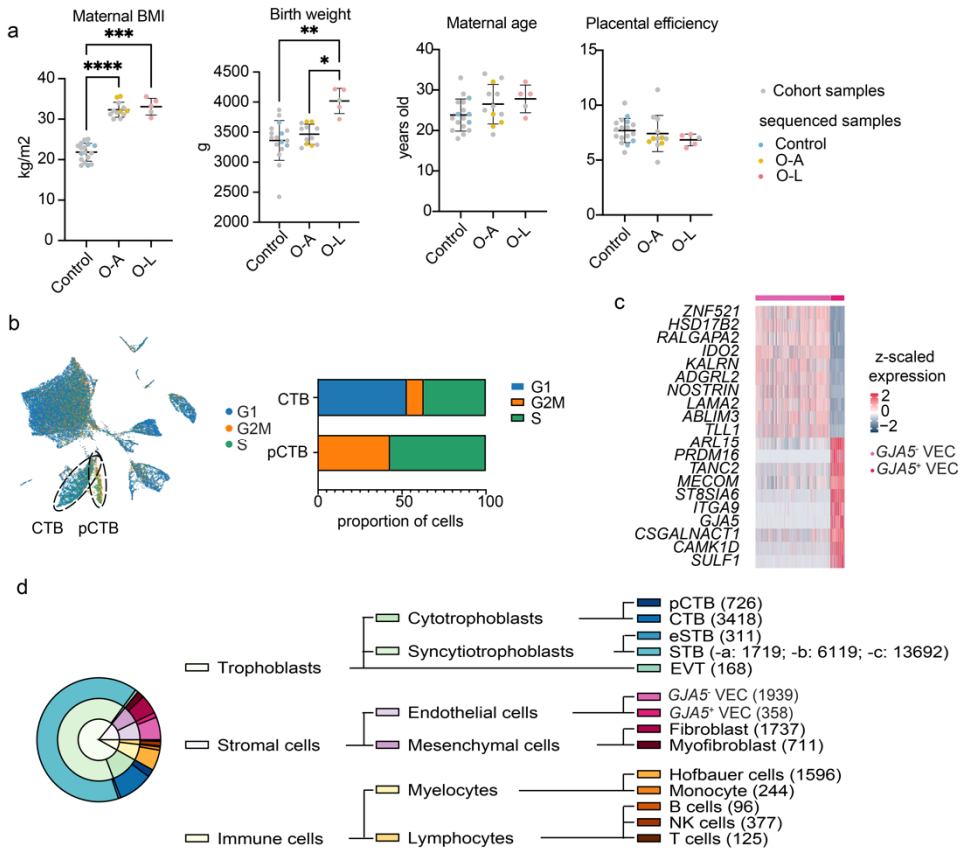

Figure S1. Single nuclei RNA-sequencing of the human placentas from normal-weighted mothers and mothers with obesity. a, Maternal BMI, birth weight, maternal age, and placental efficiency(y-axis; labeled on top of plots) in the cohort, and the samples for snRNA-seq were colored by group. **b,** Two-dimensional Uniform manifold approximation and projection (UMAP) embedding of the nuclei colored by the inferred cell cycle (left). The proportion of nuclei of CTB and pCTB in G1, G2M or S phase of cell cycle (right). **c,** The heatmap showing the gene expression of the differentially expressed genes between the two types of VEC. The color bar indicates the mean z-scored gene expression of a gene. **d,** Pie plot showing the percentage of the major cell types and their hierarchy. Total cell type number of 12 samples were written beside the cell types. Controls: normal-weighted women (n=4); O-A: Obese mother with appropriate for gestational age baby; O-L: Obese mother with large for gestational age baby; CTB: cytotrophoblasts; VEC: vascular endothelial cells; EVT: extravillous trophoblasts; pCTB: proliferative CTB; STB: syncytiotrophoblasts; eSTB: early syncytiotrophoblasts.

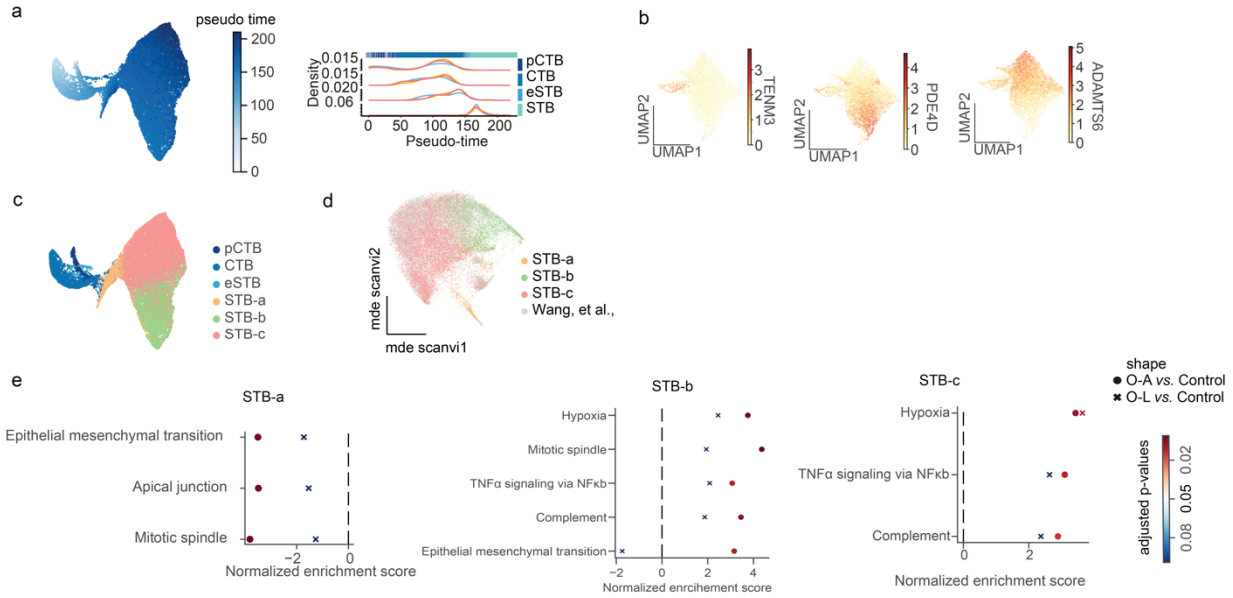

Figure S2. The three states of syncytiotrophoblast nuclei and their transcriptional response to maternal obesity. a, Two-dimensional Uniform manifold approximation and projection (UMAP) representation of villous trophoblasts colored by inferred pseudo time (left). Density plot of the cell types along pseudo time. **b,** UMAP representation of trophoblasts colored by marker genes. c, UMAP representation of trophoblasts colored by marker genes by cell types. **d,** SCANVI[40] integration of the nuclei in this study and Wang et al., colored by the labels annotated in this study. **e,** Gene set enrichment analysis[10] with the enrichment score of hallmark gene sets for O-A *vs* Control (dot) and O-L *vs* Control (cross). The shapes were colored by the Benjamini-Hochberg adjusted p-values. CTB, cytotrophoblast; pCTB, proliferative CTB; STB, syncytiotrophoblasts; eSTB, early STB.

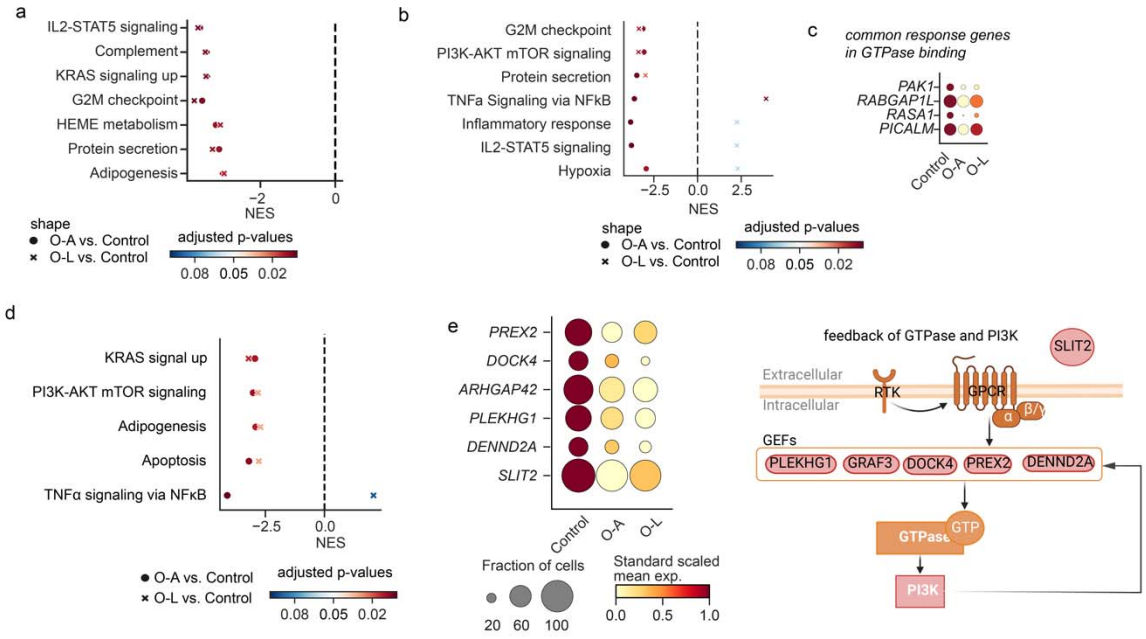

Figure S3 Transcriptional response of non-trophoblast cell types in the placentas to maternal obesity. a-b, Gene set enrichment analysis (GSEA) of the differential gene expression in O-A vs Control and O-L vs.

Control from vascular endothelial cells (a), Hofbauer cells (b). **c,** dotplot of the common regulated genes in Hofbauer cells whose ontologies include GTPase binding. **d,** GSEA of the differential gene expression in O-A vs Control and O-L vs. Control from fibroblast. **e,** (Left) dotplot of the common regulated genes in fibroblast whose ontologies include GTPase binding. (Right) illustration of the altered GTPase binding protein and PI3K signaling in fibroblast.

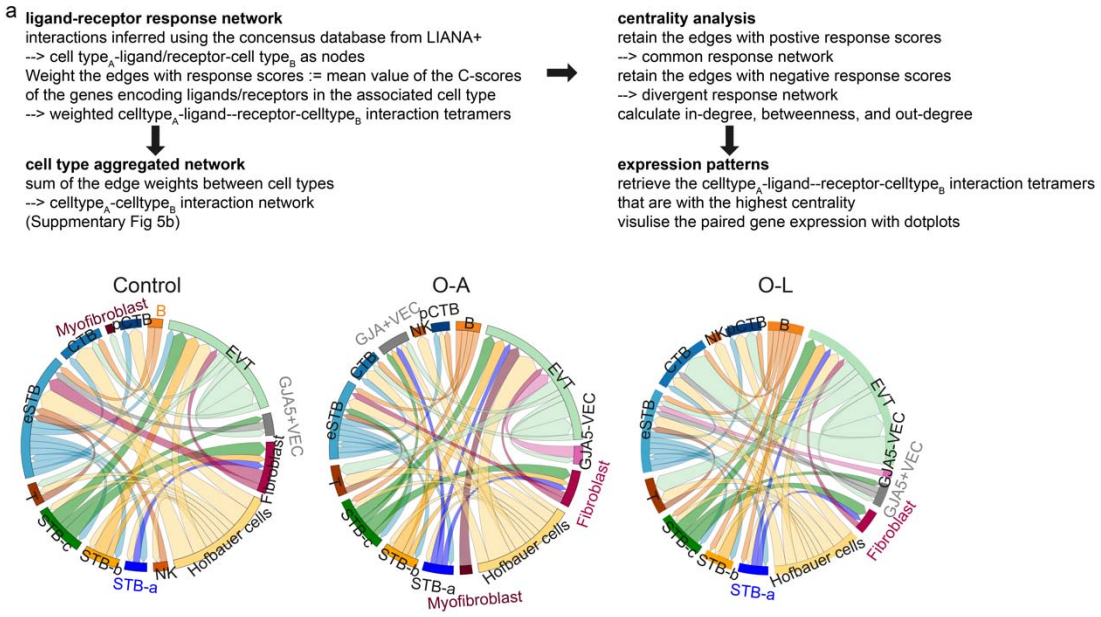

Figure S4 Communicative pathways across cell types in human placental villi. a, Procedures of cell-cell communication network analysis (top panel). And circos plot summarizing counts of ligand receptor pair between cell types generated by Liana+[77] (bottom panel).

Methods

Cohort selection

The Institutional Ethics Committee for Research on Humans of the Faculty of Medicine, University of Chile (Protocol Nr. 033-2013, 201-201, 236–2020) reviewed and approved the protocol. At the time of recruitment,

each participant received all information regarding the study, voluntarily enrolled and signed the informed consent. Women were recruited before delivery at the Maternity Service of the Hospital San Juan Dios, West Health Division, Santiago, Chile between 2014 and 2022. From the 328 placentas collected during this period, women with pregnancy complications such as hypertension, preeclampsia, thyroid disorders, GDM, preterm delivery, a fetus with malformations or chromosomal aberrations, and those with pregestational antecedents of diabetes, polycystic ovary syndrome, infertility, and assisted fertilization (IVF or ICSI) as well as those who declared to smoke, drink alcohol or take drugs during the pregnancy were excluded from this study. To the purpose of this study, women with normal pregestational weight (BMI between 18.50 -24.99 kg/m^2, n = 22) or pregestational obesity grade I (BMI between 30 – 35.7 kg/ m^2, n = 25) aged between 18 and 34 years old, that delivered from vaginal deliveries were further selected. Birth weight appropriate to gestational age (AGA) was defined as a birthweight more than 10th and below 90th percentile and birth weight large to gestational age (LGA) was defined as a birthweight above 90th percentile of the sex-specific and gestational age-specific reference mean[105]. For single-nucleus analysis, placenta samples from control (normal-weight mothers and AGA babies, n=4), O-A (mothers with obesity and AGA babies, n=4), and O-L (mothers with obesity and LGA babies, n=4) were selected. And the maternal age, height, gestational age, and baby sex were not different between groups (Figure 1f).

Statistical analysis of cohort and samples characteristics

Variables (maternal age, height and BMI, birthweight, baby size and cranial circumference, placental weight and efficiency) were analyzed using GraphPad Prism 9.4.1 for Windows (GraphPad Software, San Diego, California USA, www.graphpad.com”). For cohort comparisons, t test with Welch’s correction were applied. For snRNAseq sample data, Kruskal-Wallis test followed by two stage linear step procedure of Benjamini, Krieger and Yekutieli for adjustment were performed. For all comparisons, a variable was considered as significantly different between group for p after correction < 0.05. In the text, data are represented as mean ± SEM.

Sample collection

After delivery, placentas were collected as previously described[22] and snap frozen immediately in liquid nitrogen. Briefly, placentas from full-term pregnancies were collected immediately after delivery and processed within 30min. Each placenta was sectioned transversely using a sterile scalpel near the cord insertion site (approximately 5 cm), divided into three horizontal segments from the chorionic surface toward the basal plate and codified as S1: near to chorionic plate; S2: zone between chorionic plate and basal plate; and S3: near to basal plate. S1 Samples were subjective to analyze to avoid decidua and chorionic plate. The samples were then conserved in -80°C freezers until transport to Sweden when they were kept on dry ice and then store again in -80°C freezers. Newborn data such as sex, weight, height, and head circumference were recorded. Placental efficiency was calculated as the ratio of neonatal weight (g) to placental weight (g).

Nucleus isolation

Protocol for nucleus isolation was adapted from the protocol optimized for human placenta samples by Ludivine Doridot and her team (Institut Cochin, France). Briefly, 30mg of frozen placenta was chopped into small pieces on dry ice and added to douncer on ice with cold NP-40 lysis buffer containing RNase inhibitor. After 10min of incubation, lysis buffer was diluted in wash medium (cold PBS with 2% BSA and RNase inhibitor) and 10 strokes with the loose pestle were performed. Samples were further filtered (100µm) and centrifuged at 600g, for 5 min at 4C. Pellet was resuspended in cold wash medium, and then further filter (40µm) and centrifuged again. After resuspension in nuclei resuspension buffer (1% BSA and RNase inhibitor solution in DPBS), the pellet was filtered one last time (20µm).

The number of isolated nuclei was determined using trypan blue staining and automated cell counter (Biorad, TC20) and quality of nuclei was assessed by visualization under microscope (EVOS XL Core, ThermoFisher Scientific).

10x Genomics library preparation and sequencing

Suspension of good quality nuclei were processed as manufacturer's protocol for the Chromium Single Cell 3' kit v3.1 (10X Genomics). Library preparation was performed to obtain between 1,000 and 10,000 nuclei per reaction. Libraries were then sequenced to obtained 90GB of data (paired end, 150bp) per reaction on the Illumina NovaSeq 6000 at Novogene, UK.

snRNA-seq processing

Gene counts were obtained by aligning reads to the GRCh38 genome using Cell Ranger software (10x Genomics). We used scanpy[106] to process and cluster the expression profiles and infer cell identities of major cell classes. Cellbender[107] was used to remove background noise. In addition, using Scrublet[108], cells that were labeled as doublets were removed.

For the UMAP visualization of individual major cell type classes, the analytical Pearson residue was used to find the highly variable genes from individual batches. We selected the set of relevant principal components based on elbow plots. High resolution cell clusters were identified using the Leiden clustering algorithm. We annotated cell types using previously published marker genes and single-cell RNA-sequencing data[109].

For the Pseudo-time analysis of trophoblast nuclei, Slingshot[33] was applied. Slingshot was designed to identify a minimum spanning tree (MST). In this setting, pCTB was assigned as an initial cell state and STB was classified as a terminal cell state.

We integrate the syncytiotrophoblast data generated in this study with the syncytiotrophoblast data from the public human healthy term placenta snRNA-seq data[110] into the same embedding using scANVI[40]. We transferred their label onto our nuclei and compared the transferred labels with our labels using the sihouette metric. The silhouette metric' values range from [−1, 1] with 1 indicates distinct labels, 0 indicates overlapping labels. Thus, the absolute value of the silhouette width is used to measure how well labels are mixed.

We applied a Bayesian model in scCODA[111] for testing the compositional differences across groups. pCTB population was selected as the reference cell type, which is assumed to be unchanged in absolute abundance, and parameters inference was calculated via Hamiltonian Monte Carlo (HMC) sampling.

Differential expression of obesity groups vs. control

We performed differential expression analyses using a Wald test with a negative binomial regression model using the formula "~ 1 + group + sex + log_number_of_genes" on raw counts. Such analysis is deployed in R Seurat package[112]. By default, in FindMarkers function in Seurat, genes with more than one count in at least 1% of cells were considered. This rendered 6,000 to 7,000 genes to be analyzed. FDR was estimated with Benjamini-Hochberg method. The statistics from this analysis were used as the input in the following method section.

For the gene set enrichment analysis, we ranked the genes in O-A vs. Control and O-L vs. Control differential gene expression analysis respectively by fold changes. We then followed the GSEA[113] recommandations to get the normalized enrichment scores. Specifically, an enrichment score was calculated by walking down the list of genes, increasing a running-sum statistic when a feature in each hallmark gene set is encountered and decreasing it when it is not. The final score is the maximum deviation from zero encountered in the random walk. Finally, a normalized score was obtained by computing the z-score of the estimate compared to a null distribution obtained from N random permutations. The p-values were adjusted by the BH method[114] to control the false discovery rate.

Gene Ontology enrichment analyses were performed using Enrichr[59]. Specifically, Fisher's exact test was used to test the overrepresentation of the gene sets of interest from this study in known gene sets from MsigDB

Hallmark database. The p-value from the test was adjusted with the BH method.

Scoring the common or divergent DEGs between comparisons

To measure the similarities or differences in differential gene expression between the two obese groups and the normal weight group, we construct a score based on the fold changes of the genes and the false discovery rates (FDRs) of the two comparisons:

$$Score = Magnitude \times Ratio$$

$$Magnitude = |E1 \times wFDR_{E1}| + |E2 \times wFDR_{E2}|$$

$$Ratio = \begin{cases} \dfrac{\max(E1, E2)}{|E1 - E2| + 1}, & E1 \times E2 > 0 \\ -\dfrac{|E1 - E2|}{\max(|E1|, |E2|) + 1}, & E1 \times E2 \leq 0 \end{cases}$$

$$wFDR = \begin{cases} 1, & FDR < 0.05 \\ \dfrac{log_{10}FDR}{log_{10}0.05}, & FDR \geq 0.05 \end{cases}$$

$$E1 \coloneqq NES\ or\ log_2FC\ for\ O - A\ vs\ Control, C2 \coloneqq NES\ or\ log_2FC\ for\ O - L\ vs\ Control$$

A positive score indicates that the genes were both increased and decreased in the two comparisons. The higher the score, the more common and larger fold changes were. Conversely, a negative score indicates that the gene was oppositely expressed in the two obese groups compared to the normal weight group. This means that it was increased in one comparison group and decreased in the other. The more negative the score, the more divergent and larger fold changes the gene had. In this algorithm, genes with zero-fold changes were scored as zero.

To measure the significance of the scores of genes that were differentially expressed (score≠0), we performed a permutation test. The fold changes and FDRs of all these genes in each comparison were permuted 40,000 times if the number of genes with a score≠0 was over 200, otherwise, they were permuted $(\text{number of the genes})^2$ times. The p-values were then assigned to the observed scores as the frequencies of the permutated scores > the observed score when the observed score is positive or as frequencies of permuted scores < the observed score when the observed score is negative. A one-sided p-value < 0.05 was used for significance.

Cell-cell communication (CCC) network analysis

Ligand–receptor interactions contrasts across cell type pairs were inferred using the consensus ligand–receptor database from LIANA+[115]. The ligand-receptor edges were weighted by the sum of C-scores for the corresponding genes obtained with the method stated in the preceding section. This generated the cellA–cellB–ligand–receptor interaction tetramers weighted by the commonness of the response in the two obesity groups vs control. The mean p-values for the C-scores of the corresponding genes were assigned to the tetramers indicating significance of the interaction as a response to maternal obesity.

From the weighted CCC network, the in-degree, out-degree, and betweenness centrality were calculated.

Betweenness centrality measures the extent to which a vertex lies on paths between other vertices. Vertices with high betweenness may have considerable influence within a network by virtue of their control over information passing between others. They are also the ones whose removal from the network will most disrupt communications between other vertices because they lie on the largest number of paths taken by messages.

Adipose spheroid establishment

Adipose spheroid (AS) modeling lean and obesity conditions were established as previously described 18. Briefly, cryopreserved human primary stromal vascular fraction of white adipose tissue of female origin were seeded in culture flasks with DMEM/F-12 Glutamax, 10% FBS and 1% penicillin-streptomycin. After reaching the confluency of around 70%, cells were trypsinized and seeded into ultra-low attachment 96-well plates (Corning) with 5,000 cells per well and centrifuged at 150g for 2 min. After 4 days, the culture medium was changed to serum-free differentiation medium (*maintenance medium*, William's E supplemented with 2mM L-Glutamine, 100 units/ml penicillin, 100µg/ml streptomycin, 10µg/ml insulin, 10µg/ml transferrin, 6.7ng/ml sodium selenite and 100nM dexamethasone; *differentiation cocktail*, 500µM 3-isobutyl-1-methylxanthine (IBMX), 10nM hydrocortisone, 2nM 3,3',5-Triiodo-L-thyronine, 10µM rosiglitazone, 33µM biotin and 17µM pantothenic acid, and *free fatty acids (FFAs)*, 160µM oleic acid; 160µM palmitic acid conjugated to 10%BSA at a molar ratio of 1:5). After 48h, half of the medium was changed and subsequently every 3-4 days for 17 days. After differentiation, the spheroids were transferred into the maintenance media supplemented with FFAs for four days before the chip co-culture and the media was exchanged every 2 days to phase out the differentiation growth factors.

Trophoblast organoid culture establishment

Villous trophoblast primary cells were isolated from human placental tissue as described previously by Yang et al.[86]. Briefly, the isolated villi fragmented and washed intensely. Then, the tissue was digested with 0.2% trypsin (Alfa Aesar, J63993-09)/0.02% EDTA (Sigma-Aldrich, E9884) and 1 mg/mL collagenase V (Sigma, C9263), and further disrupted by pipetting up and down with a serological 10mL pipette, around 10-15 times. The cellular digests were combined and washed with Advanced DMEM/F12 medium (Life Technologies 12634-010), and cells were counted with a automatic cell counter (TC20 BioRad). After, the cells were pelleted and resuspended in pre-thawed Matrigel (Corning 35623). The volume of Matrigel is dependent on cell counting and on pellet size; in general, at least 10x of cell pellet volume should be used. 20µL domes of Matrigel/cells were seeded in a 48-well culture plate, and placed in an incubator at 37°C with 5% CO_2 for 3 minutes, then the plate was turned upside down so cells distribute evenly within the Matrigel domes. The domes were incubated for a total of 15 minutes before supplemented with 250µL of trophoblast organoid maintenance medium, composed with: Advanced DMEM/ F12 (Life Technologies, 12634-010); 1x B27 (Life Technologies, 17504-044); 1x N2 (Life Technologies, 17502-048); 10% FBS (Cytiva HyClone, SH30070.03); 2mM L-glutamine (Life Technologies, 35050-061); 100µg/mL Primocin (InvivoGen, antpm-1); 1,25mM NAC (SigmaAldrich, A9165), 500nM A83-01 (Tocris, 2939); 1,5µM CHIR99021 (Tocris, 4423); 50ng/mL hEGF (Gibco, PHG0314); 80g/mL human R-spondin1 (R&D systems, 4645-RS-100); 100ng/mL hFGF2 (Peprotech, 100-18C); 50ng/mL hHGF (Peprotech, 100-39); 10mM nicotinamide (Sigma-Aldrich, N0636-100G); 5µM Y-27632 (Sigma, Y0503-1MG); 2.5µM prostaglandin E2 (PGE2, R&D systems, 22- 961-0).Medium was replaced every 2-3 days. hCG was measured to ensure proliferation of trophoblast cells using professional pregnancy test strips (Gravidetstest GI29100, Medistore). Small trophoblast organoids became noticeable and positive hCG tests were obtained around 10-15 days after establishment.

Maintenance and recovery of trophoblast organoids

Passages were performed every 5-7 days, as previously described by Yang et al. and Turco et.al. Each Matrigel dome was disintegrated by pipetting the medium up and down and by scraping. Organoid suspension was washed and digested in pre-warmed StemPro Accutase (Gibco, A11105-01) with Y-27632 (Sigma, Y0503-1MG) for 10 minutes at 37°C. After carefully removing the supernatant, 200µL of Advanced DMEM/ F12 (Life Technologies, 12634-010) was added before performing mechanical dissociation by at least 200 ups and

downs, using an automatic pipette. Cell suspension was washed and resuspended in cold Matrigel, and plated into 20 µL domes with desired cell density. 250µL of trophoblast organoid maintenance medium was added, after 15 minutes of incubation at 37°C with 5% CO_2. To remove TOs from Matrigel, 250µL of Cell Recovery Solution (Corning 354253) was added to each well. The plate was incubated on ice for 45 minutes. The Matrigel domes were dissociated by pipetting up and down, the organoid/cell recovery solution was collected and centrifuged. After removing the supernatant, the organoid pellet was washed and resuspended in cold pre-thawed Matrigel. Tubes were kept on ice until the assembly of the microfluidic co-culture.

Co-culture of trophoblast organoids with adipose spheroids on a microfluidic device

To coculture obese AS with TB-Orgs, we used multilayered microfluidic devices made of off-stoichiometric thiol–ene–epoxy (OSTE+), poly(methyl methacrylate) (PMMA) and polydimethylsiloxane (PDMS). The OSTE+ parts, which hold the tissue chambers (D = 6 mm) and microfluidic channels (W= 1000 µm, H = 500 µm), were produced from OSTEMER-322 (Mercene labs, Sweden) as previously described[82]. The PDMS layer was cast and the PMMA layer was cut using a micromilling machine (Minitech Machinery Corp., USA). The AS were grown and differentiated for 17 days and washed in maintenance media before the chip culture. Between 20 to 30 AS were loaded in the first chambers of the co-culture chips and 20-30 TB-Orgs (grown for seven days after splitting) were seeded in matrigel in the second chambers of all devices. The control chips were only seeded with TB-Orgs. To mimic an obese environment, obesogenic media (previously described) was perfused at a constant flow rate of 5µL/minute using an NE-1600 SyringeSIX Programmable Multichannel Syring Pump (New Era Pump Systems Inc.). After 4 days, TB-Org were collected for RNA-extraction.

RNA extraction and sequencing of trophoblast organoids

TOs for RNAseq analysis were recovered from Matrigel using Cell Recovery Solution (Corning, 354253), as described previously. 500µL of cold TRI reagent (Sigma-Aldrich) was added and incubated on ice for 5 minutes. Then 100µL of chloroform was added, vortex mixed and centrifuged. Around 200µL of supernatant was recovered and the same volume of isopropanol was then added. The mixture was further mixed and loaded on Minicolumn (ReliaPrep RNA Miniprep, Promega). The next steps were performed following manufacturer instructions and included DNase treatment.

Prime-seq protocol was used to prepare RNA sequencing libraries as previously described[116]. Briefly, samples with 10ng/µL of extracted RNA were used for reverse transcription and pre-amplification. The cDNA was quantified using the PicoGreen dsDNA Assay Kit (ThermoFisher Scientific) and qualified using the Bioanalyzer High Sensitivity DNA chip (Agilent), before subsequent library construction using the NEBNext Ultra II FS Kit (New England Biolabs). Then the libraries were sequenced on Illumina NovaSeq 6000 at Novogene, UK at an average depth of 20 million reads per sample.

Downstream analysis of trophoblast organoid RNA sequencing

Quality of the raw data was checked using FastQC (version 0.11.9), trimmed of poly(A) tails using Cutadapt (version 4.1), before filtering using the zUMIs[117] pipeline (version 2.9.7). The filtered data was then mapped to the human genome using STAR[118] (version 2.7.10a), and reads were counted using RSubread[119] (version 2.12.0). Lowly expressed genes (count sum <50 for all samples) were filtered out before differential analysis. Differential expression analysis on RNA sequencing data was done using the DESeq2[120] package (version 1.36.0) using paired analysis. Differentially expressed genes (DEGs) were defined as adjusted p-value<0.05 and fold-change>2 or <-2.

Data availability

Raw snRNA sequencing data from the placenta tissues were deposited in EGAS50000000834 and Raw RNA

sequencing data from trophoblast organoids were deposited in EGAS50000000834. Expected Release Date: 2025/06/13 or upon acceptance of the article. The source data for Figure 1-6 were deposited in https://zenodo.org/records/14549514.

Code availability

The explanation and script for C-score calculation and is available at https://github.com/DengLab-KI/cscore. The notebooks to reproduce the presented results is available at https://github.com/DengLab-KI/obesity_paper.

References

1. Collaboration, N.C.D.R.F. (2024). Worldwide trends in underweight and obesity from 1990 to 2022: a pooled analysis of 3663 population-representative studies with 222 million children, adolescents, and adults. Lancet *403*, 1027-1050. 10.1016/S0140-6736(23)02750-2.
2. Obesity in Pregnancy: ACOG Practice Bulletin, Number 230. (2021). Obstet Gynecol *137*, e128-e144. 10.1097/AOG.0000000000004395.
3. Zhang, C.X.W., Candia, A.A., and Sferruzzi-Perri, A.N. (2024). Placental inflammation, oxidative stress, and fetal outcomes in maternal obesity. Trends Endocrinol Metab *35*, 638-647. 10.1016/j.tem.2024.02.002.
4. Zhang, T., Bian, Q., Chen, Y., Wang, X., Yu, S., Liu, S., Ji, P., Li, L., Shrestha, M., Dong, S., et al. (2021). Dissecting human trophoblast cell transcriptional heterogeneity in preeclampsia using single-cell RNA sequencing. Mol Genet Genomic Med *9*, e1730. 10.1002/mgg3.1730.
5. Yang, Y., Guo, F., Peng, Y., Chen, R., Zhou, W., Wang, H., OuYang, J., Yu, B., and Xu, Z. (2021). Transcriptomic Profiling of Human Placenta in Gestational Diabetes Mellitus at the Single-Cell Level. Front Endocrinol (Lausanne) *12*, 679582. 10.3389/fendo.2021.679582.
6. Zhou, W., Wang, H., Yang, Y., Guo, F., Yu, B., and Su, Z. (2022). Trophoblast Cell Subtypes and Dysfunction in the Placenta of Individuals with Preeclampsia Revealed by Single□Cell RNA Sequencing. Mol Cells *45*, 317-328. 10.14348/molcells.2021.0211.
7. Campbell, K.A., Colacino, J.A., Puttabyatappa, M., Dou, J.F., Elkin, E.R., Hammoud, S.S., Domino, S.E., Dolinoy, D.C., Goodrich, J.M., Loch-Caruso, R., et al. (2023). Placental cell type deconvolution reveals that cell proportions drive preeclampsia gene expression differences. Commun Biol *6*. ARTN 264
10.1038/s42003-023-04623-6.
8. Wang, M., Liu, Y., Sun, R., Liu, F., Li, J., Yan, L., Zhang, J., Xie, X., Li, D., Wang, Y., et al. (2024). Single-nucleus multi-omic profiling of human placental syncytiotrophoblasts identifies cellular trajectories during pregnancy. Nat Genet *56*, 294-305. 10.1038/s41588-023-01647-w.
9. Gude, N.M., Roberts, C.T., Kalionis, B., and King, R.G. (2004). Growth and function of the normal human placenta. Thromb Res *114*, 397-407. 10.1016/j.thromres.2004.06.038.
10. Bell, A.W., and Ehrhardt, R.A. (2002). Regulation of placental nutrient transport and implications for fetal growth. Nutr Res Rev *15*, 211-230. 10.1079/NRR200239.
11. Sajjad, M.U., Henriksen, T., Roland, M.C.P., Haugen, G., and Michelsen, T.M. (2024). Maternal body mass index, birthweight, and placental glucose metabolism: evidence for a role of placental hexokinase. Am J Obstet Gynecol *230*, 677 e671-677 e610. 10.1016/j.ajog.2023.10.043.
12. Costa, M.A. (2016). The endocrine function of human placenta: an overview. Reprod Biomed Online *32*, 14-43. 10.1016/j.rbmo.2015.10.005.
13. Hauguel-de Mouzon, S., and Guerre-Millo, M. (2006). The placenta cytokine network and inflammatory signals. Placenta *27*, 794-798. 10.1016/j.placenta.2005.08.009.
14. Newbern, D., and Freemark, M. (2011). Placental hormones and the control of maternal metabolism and fetal growth. Curr Opin Endocrinol Diabetes Obes *18*, 409-416. 10.1097/MED.0b013e32834c800d.
15. Joseph, T.T., Schuch, V., Hossack, D.J., Chakraborty, R., and Johnson, E.L. (2024). Melatonin: the placental antioxidant and anti-inflammatory. Front Immunol *15*, 1339304. 10.3389/fimmu.2024.1339304.

16. Jones, H.N., Jansson, T., and Powell, T.L. (2010). Full-Length Adiponectin Attenuates Insulin Signaling and Inhibits Insulin-Stimulated Amino Acid Transport in Human Primary Trophoblast Cells. Diabetes *59*, 1161-1170. 10.2337/db09-0824.
17. Nugrahani, A.D., Aziz, M.A., Santoso, D.P.J., Siddiq, A., Pramatirta, A.Y., Irianti, S., Pribadi, A., Anwar, A.D., and Syamsunarno, M. (2024). Adiponectin and leptin profiles among obese pregnant women with preeclampsia vs. non-preeclampsia: a systematic review and meta-analysis. Eur Rev Med Pharmacol Sci *28*, 3922-3933. 10.26355/eurrev_202407_36524.
18. Kelly, A., Chan, J., Powell, T.L., Cox, L.A., Jansson, T., and Rosario, F.J. (2023). Maternal obesity alters the placental transcriptome in a fetal sex-dependent manner. Front Cell Dev Biol *11*, 1178533. 10.3389/fcell.2023.1178533.
19. Hirschmugl, B., Desoye, G., Catalano, P., Klymiuk, I., Scharnagl, H., Payr, S., Kitzinger, E., Schliefsteiner, C., Lang, U., Wadsack, C., and Hauguel-de Mouzon, S. (2017). Maternal obesity modulates intracellular lipid turnover in the human term placenta. Int J Obes (Lond) *41*, 317-323. 10.1038/ijo.2016.188.
20. Brett, K.E., Ferraro, Z.M., Holcik, M., and Adamo, K.B. (2016). Placenta nutrient transport-related gene expression: the impact of maternal obesity and excessive gestational weight gain. J Matern Fetal Neonatal Med *29*, 1399-1405. 10.3109/14767058.2015.1049522.
21. Nogues, P., Dos Santos, E., Couturier-Tarrade, A., Berveiller, P., Arnould, L., Lamy, E., Grassin-Delyle, S., Vialard, F., and Dieudonne, M.N. (2021). Maternal Obesity Influences Placental Nutrient Transport, Inflammatory Status, and Morphology in Human Term Placenta. J Clin Endocrinol Metab *106*, e1880-e1896. 10.1210/clinem/dgaa660.
22. Ortiz, M., Sánchez, F., Alvarez, D., Flores, C., Salas-Pérez, F., Valenzuela, R., Cantin, C., Leiva, A., Crisosto, N., and Maliqueo, M. (2023). Association between maternal obesity, essential fatty acids and biomarkers of fetal liver function. Prostag Leukotr Ess *190*. ARTN 102541 10.1016/j.plefa.2023.102541.
23. Sebire, N.J., Jolly, M., Harris, J.P., Wadsworth, J., Joffe, M., Beard, R.W., Regan, L., and Robinson, S. (2001). Maternal obesity and pregnancy outcome: a study of 287,213 pregnancies in London. Int J Obes Relat Metab Disord *25*, 1175-1182. 10.1038/sj.ijo.0801670.
24. Liu, Y., Dai, W., Dai, X., and Li, Z. (2012). Prepregnancy body mass index and gestational weight gain with the outcome of pregnancy: a 13-year study of 292,568 cases in China. Arch Gynecol Obstet *286*, 905-911. 10.1007/s00404-012-2403-6.
25. Kalk, P., Guthmann, F., Krause, K., Relle, K., Godes, M., Gossing, G., Halle, H., Wauer, R., and Hocher, B. (2009). Impact of maternal body mass index on neonatal outcome. Eur J Med Res *14*, 216-222. 10.1186/2047-783x-14-5-216.
26. Richardson, B.S., Ruttinger, S., Brown, H.K., Regnault, T.R.H., and de Vrijer, B. (2017). Maternal body mass index impacts fetal-placental size at birth and umbilical cord oxygen values with implications for regulatory mechanisms. Early Hum Dev *112*, 42-47. 10.1016/j.earlhumdev.2017.06.009.
27. Dyer, J.S., Rosenfeld, C.R., Rice, J., Rice, M., and Hardin, D.S. (2007). Insulin resistance in Hispanic large-for-gestational-age neonates at birth. J Clin Endocrinol Metab *92*, 3836-3843. 10.1210/jc.2007-0079.
28. Taal, H.R., Vd Heijden, A.J., Steegers, E.A., Hofman, A., and Jaddoe, V.W. (2013). Small and large size for gestational age at birth, infant growth, and childhood overweight. Obesity (Silver Spring) *21*, 1261-1268. 10.1002/oby.20116.
29. Kuciene, R., Dulskiene, V., and Medzioniene, J. (2018). Associations between high birth weight, being large for gestational age, and high blood pressure among adolescents: a cross-sectional study. Eur J Nutr *57*, 373-381. 10.1007/s00394-016-1372-0.
30. Kiserud, T., Piaggio, G., Carroli, G., Widmer, M., Carvalho, J., Neerup Jensen, L., Giordano, D., Cecatti, J.G., Abdel Aleem, H., Talegawkar, S.A., et al. (2017). The World Health Organization Fetal Growth Charts: A Multinational Longitudinal Study of Ultrasound Biometric Measurements and Estimated Fetal Weight. PLoS Med *14*, e1002220. 10.1371/journal.pmed.1002220.
31. Derisoud, E., Jiang, H., Zhao, A., Chavatte-Palmer, P., and Deng, Q.L. (2024). Revealing the molecular landscape of human placenta: a systematic review and meta-analysis of single-cell RNA

sequencing studies. Human Reproduction Update *30*, 410-441. 10.1093/humupd/dmae006.

32. Adane, A.A., Mishra, G.D., and Tooth, L.R. (2016). Diabetes in Pregnancy and Childhood Cognitive Development: A Systematic Review. Pediatrics *137*. 10.1542/peds.2015-4234.
33. Street, K., Risso, D., Fletcher, R.B., Das, D., Ngai, J., Yosef, N., Purdom, E., and Dudoit, S. (2018). Slingshot: cell lineage and pseudotime inference for single-cell transcriptomics. Bmc Genomics *19*, 477. 10.1186/s12864-018-4772-0.
34. El-Tarhouny, S.A., Almasry, S.M., Elfayomy, A.K., Baghdadi, H., and Habib, F.A. (2014). Placental growth factor and soluble Fms-like tyrosine kinase 1 in diabetic pregnancy: A possible relation to distal villous immaturity. Histol Histopathol *29*, 259-272. 10.14670/HH-29.259.
35. Nonn, O., Debnath, O., Valdes, D.S., Sallinger, K., Secener, A.K., Haider, S., Fischer, C., Tiesmeyer, S., Nimo, J., Kuenzer, T., et al. (2022). Disturbed trophoblast transition links preeclampsia progression from placenta to the maternal syndrome. bioRxiv, 2022.2010.2010.511539. 10.1101/2022.10.10.511539.
36. Gerbaud, P., Tasken, K., and Pidoux, G. (2015). Spatiotemporal regulation of cAMP signaling controls the human trophoblast fusion. Front Pharmacol *6*, 202. 10.3389/fphar.2015.00202.
37. Cain, S.A., Mularczyk, E.J., Singh, M., Massam-Wu, T., and Kielty, C.M. (2016). ADAMTS-10 and -6 differentially regulate cell-cell junctions and focal adhesions. Sci Rep *6*, 35956. 10.1038/srep35956.
38. Keenen, M.M., Yang, L., Liang, H., Farmer, V.J., Singh, R., Gladfelter, A.S., and Coyne, C.B. (2024). Comparative analysis of the syncytiotrophoblast in placenta tissue and trophoblast organoids using snRNA sequencing. bioRxiv. 10.1101/2024.07.01.601571.
39. Coleman, S.J., Gerza, L., Jones, C.J., Sibley, C.P., Aplin, J.D., and Heazell, A.E. (2013). Syncytial nuclear aggregates in normal placenta show increased nuclear condensation, but apoptosis and cytoskeletal redistribution are uncommon. Placenta *34*, 449-455. 10.1016/j.placenta.2013.02.007.
40. Xu, C., Lopez, R., Mehlman, E., Regier, J., Jordan, M.I., and Yosef, N. (2021). Probabilistic harmonization and annotation of single-cell transcriptomics data with deep generative models. Mol Syst Biol *17*, e9620. 10.15252/msb.20209620.
41. Liberzon, A., Birger, C., Thorvaldsdottir, H., Ghandi, M., Mesirov, J.P., and Tamayo, P. (2015). The Molecular Signatures Database (MSigDB) hallmark gene set collection. Cell Syst *1*, 417-425. 10.1016/j.cels.2015.12.004.
42. Bakker, W.J., Harris, I.S., and Mak, T.W. (2007). FOXO3a is activated in response to hypoxic stress and inhibits HIF1-induced apoptosis via regulation of CITED2. Mol Cell *28*, 941-953. 10.1016/j.molcel.2007.10.035.
43. Brandstetter, B., Dalwigk, K., Platzer, A., Niederreiter, B., Kartnig, F., Fischer, A., Vladimer, G.I., Byrne, R.A., Sevelda, F., Holinka, J., et al. (2019). FOXO3 is involved in the tumor necrosis factor-driven inflammatory response in fibroblast-like synoviocytes. Lab Invest *99*, 648-658. 10.1038/s41374-018-0184-7.
44. Premkumar, D.R., Adhikary, G., Overholt, J.L., Simonson, M.S., Cherniack, N.S., and Prabhakar, N.R. (2000). Intracellular pathways linking hypoxia to activation of c-fos and AP-1. Adv Exp Med Biol *475*, 101-109. 10.1007/0-306-46825-5_10.
45. Ray, N., Kuwahara, M., Takada, Y., Maruyama, K., Kawaguchi, T., Tsubone, H., Ishikawa, H., and Matsuo, K. (2006). c-Fos suppresses systemic inflammatory response to endotoxin. Int Immunol *18*, 671-677. 10.1093/intimm/dxl004.
46. Jansson, T., Wennergren, M., and Illsley, N.P. (1993). Glucose transporter protein expression in human placenta throughout gestation and in intrauterine growth retardation. J Clin Endocrinol Metab *77*, 1554-1562. 10.1210/jcem.77.6.8263141.
47. Lok, C.N., and Ponka, P. (1999). Identification of a hypoxia response element in the transferrin receptor gene. J Biol Chem *274*, 24147-24152. 10.1074/jbc.274.34.24147.
48. Uhlen, M., Karlsson, M.J., Hober, A., Svensson, A.S., Scheffel, J., Kotol, D., Zhong, W., Tebani, A., Strandberg, L., Edfors, F., et al. (2019). The human secretome. Sci Signal *12*. 10.1126/scisignal.aaz0274.
49. Yu, Y., He, J.H., Hu, L.L., Jiang, L.L., Fang, L., Yao, G.D., Wang, S.J., Yang, Q., Guo, Y., Liu, L., et al. (2020). Placensin is a glucogenic hormone secreted by human placenta. Embo Rep *21*, e49530. 10.15252/embr.201949530.

50. Brosens, I., Pijnenborg, R., Vercruysse, L., and Romero, R. (2011). The "Great Obstetrical Syndromes" are associated with disorders of deep placentation. Am J Obstet Gynecol *204*, 193-201. 10.1016/j.ajog.2010.08.009.
51. Sedlmayr, P., Blaschitz, A., and Stocker, R. (2014). The role of placental tryptophan catabolism. Front Immunol *5*, 230. 10.3389/fimmu.2014.00230.
52. Winship, A., Correia, J., Krishnan, T., Menkhorst, E., Cuman, C., Zhang, J.G., Nicola, N.A., and Dimitriadis, E. (2015). Blocking Endogenous Leukemia Inhibitory Factor During Placental Development in Mice Leads to Abnormal Placentation and Pregnancy Loss. Sci Rep *5*, 13237. 10.1038/srep13237.
53. Degerman, E., Ahmad, F., Chung, Y.W., Guirguis, E., Omar, B., Stenson, L., and Manganiello, V. (2011). From PDE3B to the regulation of energy homeostasis. Curr Opin Pharmacol *11*, 676-682. 10.1016/j.coph.2011.09.015.
54. Sato, S., Fujita, N., and Tsuruo, T. (2000). Modulation of Akt kinase activity by binding to Hsp90. Proc Natl Acad Sci U S A *97*, 10832-10837. 10.1073/pnas.170276797.
55. Roy, S.K., Srivastava, R.K., and Shankar, S. (2010). Inhibition of PI3K/AKT and MAPK/ERK pathways causes activation of FOXO transcription factor, leading to cell cycle arrest and apoptosis in pancreatic cancer. J Mol Signal *5*, 10. 10.1186/1750-2187-5-10.
56. Bouchard, C., Marquardt, J., Bras, A., Medema, R.H., and Eilers, M. (2004). Myc-induced proliferation and transformation require Akt-mediated phosphorylation of FoxO proteins. Embo J *23*, 2830-2840. 10.1038/sj.emboj.7600279.
57. Fock, V., Plessl, K., Fuchs, R., Dekan, S., Milla, S.K., Haider, S., Fiala, C., Knöfler, M., and Pollheimer, J. (2015). Trophoblast subtype-specific EGFR/ERBB4 expression correlates with cell cycle progression and hyperplasia in complete hydatidiform moles. Human Reproduction *30*, 789-799. 10.1093/humrep/dev027.
58. Leach, R.E., Kilburn, B.A., Petkova, A., Romero, R., and Armant, R. (2008). Diminished survival of human cytotrophoblast cells exposed to hypoxia/reoxygenation injury and associated reduction of heparin-binding epidermal growth factor-like growth factor. American Journal of Obstetrics and Gynecology *198*. ARTN 471.e1
10.1016/j.ajog.2008.01.009.
59. Lachmann, A., Torre, D., Keenan, A.B., Jagodnik, K.M., Lee, H.J., Wang, L., Silverstein, M.C., and Ma'ayan, A. (2018). Massive mining of publicly available RNA-seq data from human and mouse. Nature Communications *9*. ARTN 1366
10.1038/s41467-018-03751-6.
60. Binder, J.X., Pletscher-Frankild, S., Tsafou, K., Stolte, C., O'Donoghue, S.I., Schneider, R., and Jensen, L.J. (2014). COMPARTMENTS: unification and visualization of protein subcellular localization evidence. Database-Oxford. ARTN bau012
10.1093/database/bau012.
61. Shibuya, M. (2006). Vascular endothelial growth factor receptor-1 (VEGFR-1/Flt-1): a dual regulator for angiogenesis. Angiogenesis *9*, 225-230; discussion 231. 10.1007/s10456-006-9055-8.
62. Gerber, H.P., and Ferrara, N. (2003). The role of VEGF in normal and neoplastic hematopoiesis. J Mol Med (Berl) *81*, 20-31. 10.1007/s00109-002-0397-4.
63. Cursiefen, C., Chen, L., Borges, L.P., Jackson, D., Cao, J., Radziejewski, C., D'Amore, P.A., Dana, M.R., Wiegand, S.J., and Streilein, J.W. (2004). VEGF-A stimulates lymphangiogenesis and hemangiogenesis in inflammatory neovascularization via macrophage recruitment. J Clin Invest *113*, 1040-1050. 10.1172/JCI20465.
64. Chen, T., Song, P., He, M., Rui, S., Duan, X., Ma, Y., Armstrong, D.G., and Deng, W. (2023). Sphingosine-1-phosphate derived from PRP-Exos promotes angiogenesis in diabetic wound healing via the S1PR1/AKT/FN1 signalling pathway. Burns Trauma *11*, tkad003. 10.1093/burnst/tkad003.
65. Wu, H., Liu, K., and Zhang, J. (2021). Excess fibronectin 1 participates in pathogenesis of pre-eclampsia by promoting apoptosis and autophagy in vascular endothelial cells. Mol Hum Reprod *27*. 10.1093/molehr/gaab030.
66. Dyer, L.A., and Rugonyi, S. (2021). Fetal Blood Flow and Genetic Mutations in Conotruncal Congenital Heart Disease. J Cardiovasc Dev Dis *8*. ARTN 90

10.3390/jcdd8080090.
67. Zulu, M.Z., Martinez, F.O., Gordon, S., and Gray, C.M. (2019). The Elusive Role of Placental Macrophages: The Hofbauer Cell. J Innate Immun *11*, 447-456. 10.1159/000497416.
68. Shen, X.B., Chen, X., Zhang, Z.Y., Wu, F.F., and Liu, X.H. (2021). Cathepsin C inhibitors as anti-inflammatory drug discovery: Challenges and opportunities. Eur J Med Chem *225*, 113818. 10.1016/j.ejmech.2021.113818.
69. Zannas, A.S., Jia, M.W., Hafner, K., Baumert, J., Wiechmann, T., Pape, J.C., Arloth, J., Ködel, M., Martinelli, S., Roitman, M., et al. (2019). Epigenetic upregulation of FKBP5 by aging and stress contributes to NF-κB-driven inflammation and cardiovascular risk. P Natl Acad Sci USA *116*, 11370-11379. 10.1073/pnas.1816847116.
70. Ognjanovic, S., and Bryant-Greenwood, G.D. (2002). Pre-B-cell colony-enhancing factor, a novel cytokine of human fetal membranes. American Journal of Obstetrics and Gynecology *187*, 1051-1058. 10.1067/mob.2002.126295.
71. Zernichow, L., Åbrink, M., Hallgren, J., Grujic, M., Pejler, G., and Kolset, S.O. (2006). Serglycin is the major secreted proteoglycan in macrophages and has a role in the regulation of macrophage tumor necrosis factor-α secretion in response to lipopolysaccharide. J Biol Chem *281*, 26792-26801. 10.1074/jbc.M512889200.
72. Hofer, T.P.J., Frankenberger, M., Mages, J., Lang, R., Hoffmann, R., Colige, A., and Ziegler-Heitbrock, L. (2008). Tissue-specific induction of ADAMTS2 in monocytes and macrophages by glucocorticoids. J Mol Med *86*, 323-332. 10.1007/s00109-007-0284-0.
73. Turco, M.Y., and Moffett, A. (2019). Development of the human placenta. Development *146*. ARTN dev163428
10.1242/dev.163428.
74. Campa, C.C., Ciraolo, E., Ghigo, A., Germena, G., and Hirsch, E. (2015). Crossroads of PI3K and Rac pathways. Small GTPases *6*, 71-80. 10.4161/21541248.2014.989789.
75. Zhang, X.B., Tang, N.M., Hadden, T.J., and Rishi, A.K. (2011). Akt, FoxO and regulation of apoptosis. Bba-Mol Cell Res *1813*, 1978-1986. 10.1016/j.bbamcr.2011.03.010.
76. Alikhani, M., Alikhani, Z., and Graves, D.T. (2005). FOXO1 functions as a master switch that regulates gene expression necessary for tumor necrosis factor-induced fibroblast apoptosis. J Biol Chem *280*, 12096-12102. 10.1074/jbc.M412171200.
77. Dimitrov, D., Schäfer, P.S.L., Farr, E., Rodriguez-Mier, P., Lobentanzer, S., Badia-i-Mompel, P., Dugourd, A., Tanevski, J., Flores, R.O.R., and Saez-Rodriguez, J. (2024). LIANA plus provides an all-in-one framework for cell-cell communication inference. Nat Cell Biol. 10.1038/s41556-024-01469-w.
78. Maruo, T., Matsuo, H., Murata, K., and Mochizuki, M. (1992). Gestational Age-Dependent Dual Action of Epidermal Growth-Factor on Human Placenta Early in Gestation. J Clin Endocr Metab *75*, 1362-1367. DOI 10.1210/jc.75.5.1362.
79. Faxén, M., Nasiell, J., Blanck, A., Nisell, H., and Lunell, N.O. (1998). Altered mRNA expression pattern of placental epidermal growth factor receptor (EGFR) in pregnancies complicated by preeclampsia and/or intrauterine growth retardation. Am J Perinat *15*, 9-13. DOI 10.1055/s-2007-993890.
80. Jaitin, D.A., Adlung, L., Thaiss, C.A., Weiner, A., Li, B.G., Descamps, H., Lundgren, P., Bleriot, C., Liu, Z.Y., Deczkowska, A., et al. (2019). Lipid-Associated Macrophages Control Metabolic Homeostasis in a Trem2-Dependent Manner. Cell *178*, 686-+. 10.1016/j.cell.2019.05.054.
81. Zucker, S., Drews, M., Conner, C., Foda, H.D., DeClerck, Y.A., Langley, K.E., Bahou, W.F., Docherty, A.J., and Cao, J. (1998). Tissue inhibitor of metalloproteinase-2 (TIMP-2) binds to the catalytic domain of the cell surface receptor, membrane type 1-matrix metalloproteinase 1 (MT1-MMP). J Biol Chem *273*, 1216-1222. 10.1074/jbc.273.2.1216.
82. Shafagh, R.Z., Youhanna, S., Keulen, J., Shen, J.X., Taebnia, N., Preiss, L.C., Klein, K., Büttner, F.A., Bergqvist, M., van der Wijngaart, W., and Lauschke, V.M. (2022). Bioengineered Pancreas-Liver Crosstalk in a Microfluidic Coculture Chip Identifies Human Metabolic Response Signatures in Prediabetic Hyperglycemia. Adv Sci *9*. 10.1002/advs.202203368.
83. Shen, J.X., Couchet, M., Dufau, J., Barbosa, T.D., Ulbrich, M.H., Helmstädter, M., Kemas, A.M., Shafagh, R.Z., Marques, M.A., Hansen, J.B., et al. (2021). 3D Adipose Tissue Culture Links the

Organotypic Microenvironment to Improved Adipogenesis. Adv Sci *8*. ARTN 2100106 10.1002/advs.202100106.

84. Turco, M.Y., Gardner, L., Kay, R.G., Hamilton, R.S., Prater, M., Hollinshead, M.S., McWhinnie, A., Esposito, L., Fernando, R., Skelton, H., et al. (2018). Trophoblast organoids as a model for maternal-fetal interactions during human placentation. Nature *564*, 263-+. 10.1038/s41586-018-0753-3.
85. Yang, L., Semmes, E.C., Ovies, C., Megli, C., Permar, S., Gilner, J.B., and Coyne, C.B. (2022). Innate immune signaling in trophoblast and decidua organoids defines differential antiviral defenses at the maternal-fetal interface. Elife *11*. 10.7554/eLife.79794.
86. Cameo, P., Bischof, P., and Calvo, J.C. (2003). Effect of leptin on progesterone, human chorionic gonadotropin, and interleukin-6 secretion by human term trophoblast cells in culture. Biol Reprod *68*, 472-477. 10.1095/biolreprod.102.006122.
87. Farah, N., Hogan, A.E., O'Connor, N., Kennelly, M.M., O'Shea, D., and Turner, M.J. (2012). Correlation between maternal inflammatory markers and fetomaternal adiposity. Cytokine *60*, 96-99. 10.1016/j.cyto.2012.05.024.
88. Radaelli, T., Uvena-Celebrezze, J., Minium, J., Huston-Presley, L., Catalano, P., and Hauguel-de Mouzon, S. (2006). Maternal interleukin-6: Marker of fetal growth and adiposity. J Soc Gynecol Invest *13*, 53-57. 10.1016/j.jsgi.2005.10.003.
89. Challier, J.C., Basu, S., Bintein, T., Minium, J., Hotmire, K., Catalano, P.M., and Mouzon, S.H.D. (2008). Obesity in pregnancy stimulates macrophage accumulation and inflammation in the placenta. Placenta *29*, 274-281. 10.1016/j.placenta.2007.12.010.
90. Varastehpour, A., Radaelli, T., Minium, J., Ortega, H., Herrera, E., Catalano, P., and Hauguel-de Mouzon, S. (2006). \Activation of phospholipase A2 is associated with generation of placental lipid signals and fetal obesity. J Clin Endocr Metab *91*, 248-255. 10.1210/jc.2005-0873.
91. Jansson, N., Nilsfelt, A., Gellerstedt, M., Wennergren, M., Rossander-Hulthén, L., Powell, T.L., and Jansson, T. (2008). Maternal hormones linking maternal body mass index and dietary intake to birth weight. Am J Clin Nutr *87*, 1743-1749. DOI 10.1093/ajcn/87.6.1743.
92. Bhaumick, B., George, D., and Bala, R.M. (1992). Potentiation of Epidermal Growth Factor-Induced Differentiation of Cultured Human Placental Cells by Insulin-Like Growth Factor-I. J Clin Endocr Metab *74*, 1005-1011. DOI 10.1210/jc.74.5.1005.
93. Kniss, D.A., Shubert, P.J., Zimmerman, P.D., Landon, M.B., and Gabbe, S.G. (1994). Insulin-Like Growth-Factors - Their Regulation of Glucose and Amino-Acid-Transport in Placental Trophoblasts Isolated from First-Trimester Chorionic Villi. J Reprod Med *39*, 249-256.
94. Ramsay, J.E., Ferrell, W.R., Crawford, L., Wallace, A.M., Greer, I.A., and Sattar, N. (2002). Maternal obesity is associated with dysregulation of metabolic, vascular, and inflammatory pathways. J Clin Endocrinol Metab *87*, 4231-4237. 10.1210/jc.2002-020311.
95. Kawai, T., Autieri, M.V., and Scalia, R. (2021). Adipose tissue inflammation and metabolic dysfunction in obesity. Am J Physiol Cell Physiol *320*, C375-C391. 10.1152/ajpcell.00379.2020.
96. Audrito, V., Messana, V.G., and Deaglio, S. (2020). NAMPT and NAPRT: Two Metabolic Enzymes With Key Roles in Inflammation. Front Oncol *10*. ARTN 358 10.3389/fonc.2020.00358.
97. Zhang, P., Miska, J., and Heimberger, A.B. (2023). GLUT3 regulates alternative macrophage signaling through a glucose transport-independent role. J Clin Invest *133*. 10.1172/JCI174540.
98. Bill, R., Wirapati, P., Messemaker, M., Roh, W., Zitti, B., Duval, F., Kiss, M., Park, J.C., Saal, T.M., Hoelzl, J., et al. (2023). CXCL9:SPP1 macrophage polarity identifies a network of cellular programs that control human cancers. Science *381*, 515-524. 10.1126/science.ade2292.
99. Bezemer, R.E., Faas, M.M., van Goor, H., Gordijn, S.J., and Prins, J.R. (2024). Decidual macrophages and Hofbauer cells in fetal growth restriction. Front Immunol *15*. ARTN 1379537 10.3389/fimmu.2024.1379537.
100. Loegl, J., Hiden, U., Nussbaumer, E., Schliefsteiner, C., Cvitic, S., Lang, I., Wadsack, C., Huppertz, B., and Desoye, G. (2016). Hofbauer cells of M2a, M2b and M2c polarization may regulate feto-placental angiogenesis. Reproduction *152*, 447-455. 10.1530/Rep-16-0159.
101. Goudreau, A.D., Everest, C., Tanara, L., Tzaneva, V., and Adamo, K.B. (2023). Characterization of Hofbauer cell polarization and VEGF localization in human term placenta from active and inactive

pregnant individuals. Physiological Reports *11*. ARTN e15741 10.14814/phy2.15741.

102. Hashimoto, R., Sakai, K., Matsumoto, H., and Iwashita, M. (2010). Tumor Necrosis Factor-α (TNF-α) Inhibits Insulin-like Growth Factor-I (IGF-I) Activities in Human Trophoblast Cell Cultures Through IGF-I/Insulin Hybrid Receptors. Endocr J *57*, 193-200. DOI 10.1507/endocrj.K09E-189.

103. Hoeft, K., Schaefer, G.J.L., Kim, H., Schumacher, D., Bleckwehl, T., Long, Q., Klinkhammer, B.M., Peisker, F., Koch, L., Nagai, J., et al. (2023). Platelet-instructed SPP1(+) macrophages drive myofibroblast activation in fibrosis in a CXCL4-dependent manner. Cell Rep *42*, 112131. 10.1016/j.celrep.2023.112131.

104. Mallapaty, S. (2024). Human embryo models are getting more realistic - raising ethical questions. Nature *633*, 268-271. 10.1038/d41586-024-02915-3.

105. (!!! INVALID CITATION !!! 22).

106. Wolf, F.A., Angerer, P., and Theis, F.J. (2018). SCANPY: large-scale single-cell gene expression data analysis. Genome Biology *19*. ARTN 15 10.1186/s13059-017-1382-0.

107. Fleming, S.J., Chaffin, M.D., Arduini, A., Akkad, A.D., Banks, E., Marioni, J.C., Philippakis, A.A., Ellinor, P.T., and Babadi, M. (2023). Unsupervised removal of systematic background noise from droplet-based single-cell experiments using CellBender. Nat Methods *20*, 1323-+. 10.1038/s41592-023-01943-7.

108. Wolock, S.L., Lopez, R., and Klein, A.M. (2019). Scrublet: Computational Identification of Cell Doublets in Single-Cell Transcriptomic Data. Cell Syst *8*, 281-+. 10.1016/j.cels.2018.11.005.

109. Derisoud, E., Jiang, H., Zhao, A., Chavatte-Palmer, P., and Deng, Q. (2024). Revealing the molecular landscape of human placenta: a systematic review and meta-analysis of single-cell RNA sequencing studies. Hum Reprod Update *30*, 410-441. 10.1093/humupd/dmae006.

110. (!!! INVALID CITATION !!! 20).

111. Buttner, M., Ostner, J., Muller, C.L., Theis, F.J., and Schubert, B. (2021). scCODA is a Bayesian model for compositional single-cell data analysis. Nat Commun *12*, 6876. 10.1038/s41467-021-27150-6.

112. Butler, A., Hoffman, P., Smibert, P., Papalexi, E., and Satija, R. (2018). Integrating single-cell transcriptomic data across different conditions, technologies, and species. Nat Biotechnol *36*, 411-+. 10.1038/nbt.4096.

113. Subramanian, A., Tamayo, P., Mootha, V.K., Mukherjee, S., Ebert, B.L., Gillette, M.A., Paulovich, A., Pomeroy, S.L., Golub, T.R., Lander, E.S., and Mesirov, J.P. (2005). Gene set enrichment analysis: a knowledge-based approach for interpreting genome-wide expression profiles. Proc Natl Acad Sci U S A *102*, 15545-15550. 10.1073/pnas.0506580102.

114. Benjamini, Y., and Hochberg, Y. (1995). Controlling the False Discovery Rate - a Practical and Powerful Approach to Multiple Testing. J R Stat Soc B *57*, 289-300. DOI 10.1111/j.2517-6161.1995.tb02031.x.

115. Dimitrov, D., Schäfer, P.S.L., Farr, E., Rodriguez-Mier, P., Lobentanzer, S., Badia-i-Mompel, P., Dugourd, A., Tanevski, J., Flores, R.O.R., and Saez-Rodriguez, J. (2024). LIANA plus provides an all-in-one framework for cell-cell communication inference. Nat Cell Biol *26*. 10.1038/s41556-024-01469-w.

116. Janjic, A., Wange, L.E., Bagnoli, J.W., Geuder, J., Nguyen, P., Richter, D., Vieth, B., Vick, B., Jeremias, I., Ziegenhain, C., et al. (2022). Prime-seq, efficient and powerful bulk RNA sequencing. Genome Biol *23*, 88. 10.1186/s13059-022-02660-8.

117. Parekh, S., Ziegenhain, C., Vieth, B., Enard, W., and Hellmann, I. (2018). zUMIs - A fast and flexible pipeline to process RNA sequencing data with UMIs. Gigascience *7*. 10.1093/gigascience/giy059.

118. Dobin, A., Davis, C.A., Schlesinger, F., Drenkow, J., Zaleski, C., Jha, S., Batut, P., Chaisson, M., and Gingeras, T.R. (2013). STAR: ultrafast universal RNA-seq aligner. Bioinformatics *29*, 15-21. 10.1093/bioinformatics/bts635.

119. Liao, Y., Smyth, G.K., and Shi, W. (2019). The R package Rsubread is easier, faster, cheaper and better for alignment and quantification of RNA sequencing reads. Nucleic Acids Res *47*, e47. 10.1093/nar/gkz114.

120. Love, M.I., Huber, W., and Anders, S. (2014). Moderated estimation of fold change and dispersion for RNA-seq data with DESeq2. Genome Biol *15*, 550. 10.1186/s13059-014-0550-8.

Acknowledgements

Thank you to Ludivine Doridot, Céline Méhats, Vaarany Karunanith and the CYBIO core facility from the Cochin Institute for the nucleus extraction protocol. We further thank Ludivine Doridot for the good advice that she gave us for the placental nuclei extraction. The mapping of the sequencing data and ambient removal were enabled by resources provided by the National Academic Infrastructure for Supercomputing in Sweden (NAISS), partially funded by the Swedish Research Council through grant agreement no. 2022-06725.

Author contributions

H.J contributed to the conception of the work, analysis, and interpretation of data, the formulation of the C-score used in this work, and have drafted the work; E.D contributed to the design of the work, the acquisition of the data, and have revised the work; D.P contributed to the acquisition of the trophoblast organoids data and have revised the work; N.T contributed to the acquisition of the adipose spheroids and microfluidic co-culture system; R.Z.S fabricated and characterized the microfluidic devices; M.O contributed the acquisition of the placental tissues; P.R.J contributed to the acquisition of the trophoblast organoids; A.Z contributed to revise the work; C.L contributed to the library construction the placental tissues; M.A.M contributed to the acquisition of the placental tissues; E.S-V contributed to the design of the work and the acquisition of the samples; V.M.L contributed to the acquisition of adipose spheroids and microfluidic co-culture system; Q.D contributed to the design of the work, acquisition of the placental tissues, interpretation of the data, and revised this work. All authors contributed to drafting and revising the manuscript.

Funding

Supported by the Swedish Medical Research Council: project nos. 2018-02557(Q.D.), 2020-00253(Q.D.) and 2022-00550 (E.S.-V.), 2021-02801 (V.M.L.), 2023-03015 (V.M.L.) and 2024-03401 (V.M.L.); the Knut and Alice Wallenberg Foundation: 2019.0211 (Q.D.) and VC-2021-0026 (V.M.L.); Karolinska Instiutet faculty funded position (Q.D.); Diabetes foundation: DIA2022-733 (Q.D.); Barndiabetesfonden (Q.D.); Distinguished Investigator Grant – Endocrinology and Metabolism, Novo Nordisk Foundation: NNF22OC0072904 (E.S.-V.); the Diabetes Foundation: DIA2021-633 (E.S.-V.); the Karolinska Institutet-China scholarship council program (H.J.); the Robert Bosch Foundation (V.M.L.), as well as the Innovative Medicines Initiative 2 Joint Undertaking (JU) under grant agreement No. 875510 (V.M.L.).

Declaration of Competing Interests

V.M.L. is co-founder, CEO and shareholder of HepaPredict AB, as well as co-founder and shareholder of Shanghai Hepo Biotechnology Ltd. The other authors declare no competing interests.